The North Atlantic Oscillation

- characteristics
- climate impacts
- stratospheric origin
- ocean response
- coupled processes

Teleconnectivity of the atmosphere: PNA and NAO

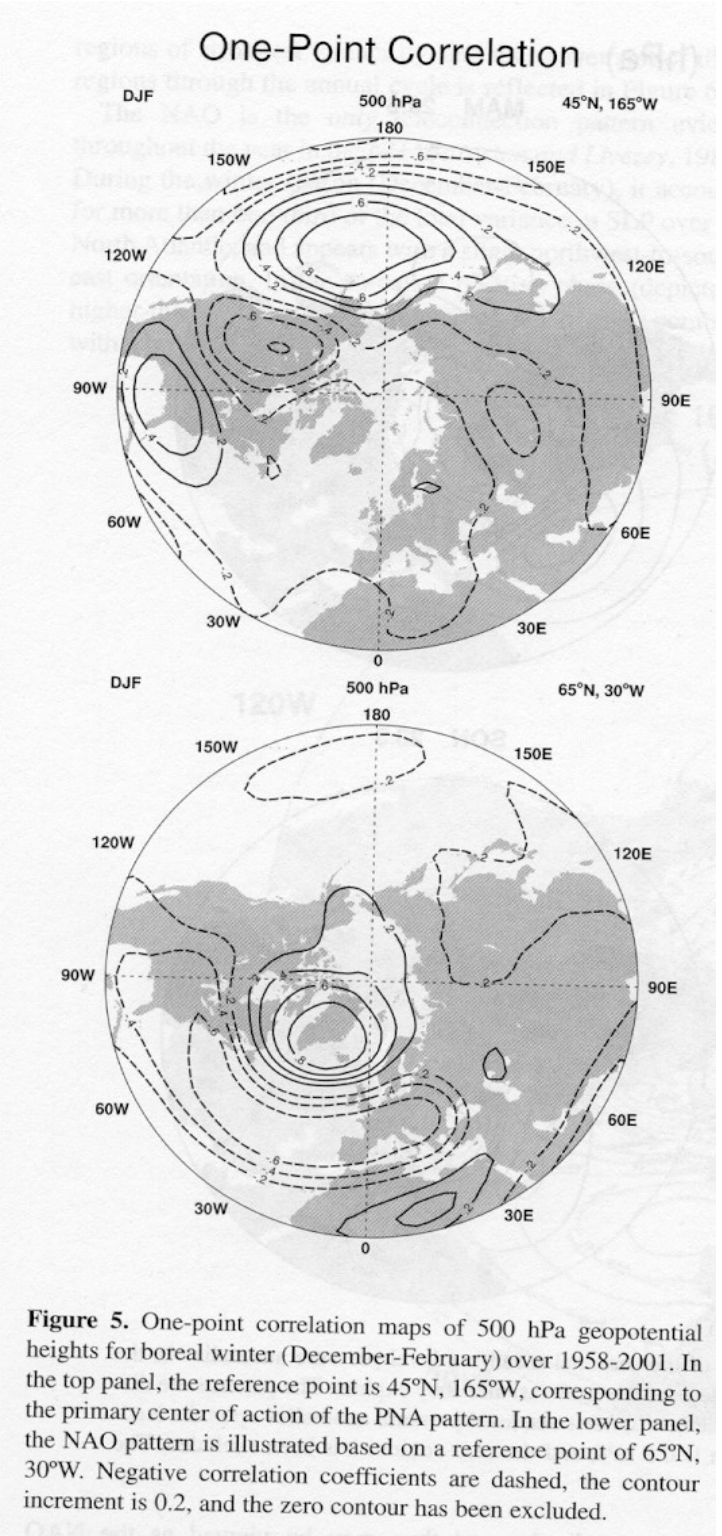

Figure 5. One-point correlation maps of 500 hPa geopotential heights for boreal winter (December-February) over 1958-2001. In the top panel, the reference point is 45°N, 165°W, corresponding to the primary center of action of the PNA pattern. In the lower panel, the NAO pattern is illustrated based on a reference point of 65°N, 30°W. Negative correlation coefficients are dashed, the contour increment is 0.2, and the zero contour has been excluded.

PNA

NAO

Hurrell et al. 2003

NAO: year round phenomenon strongest in winter

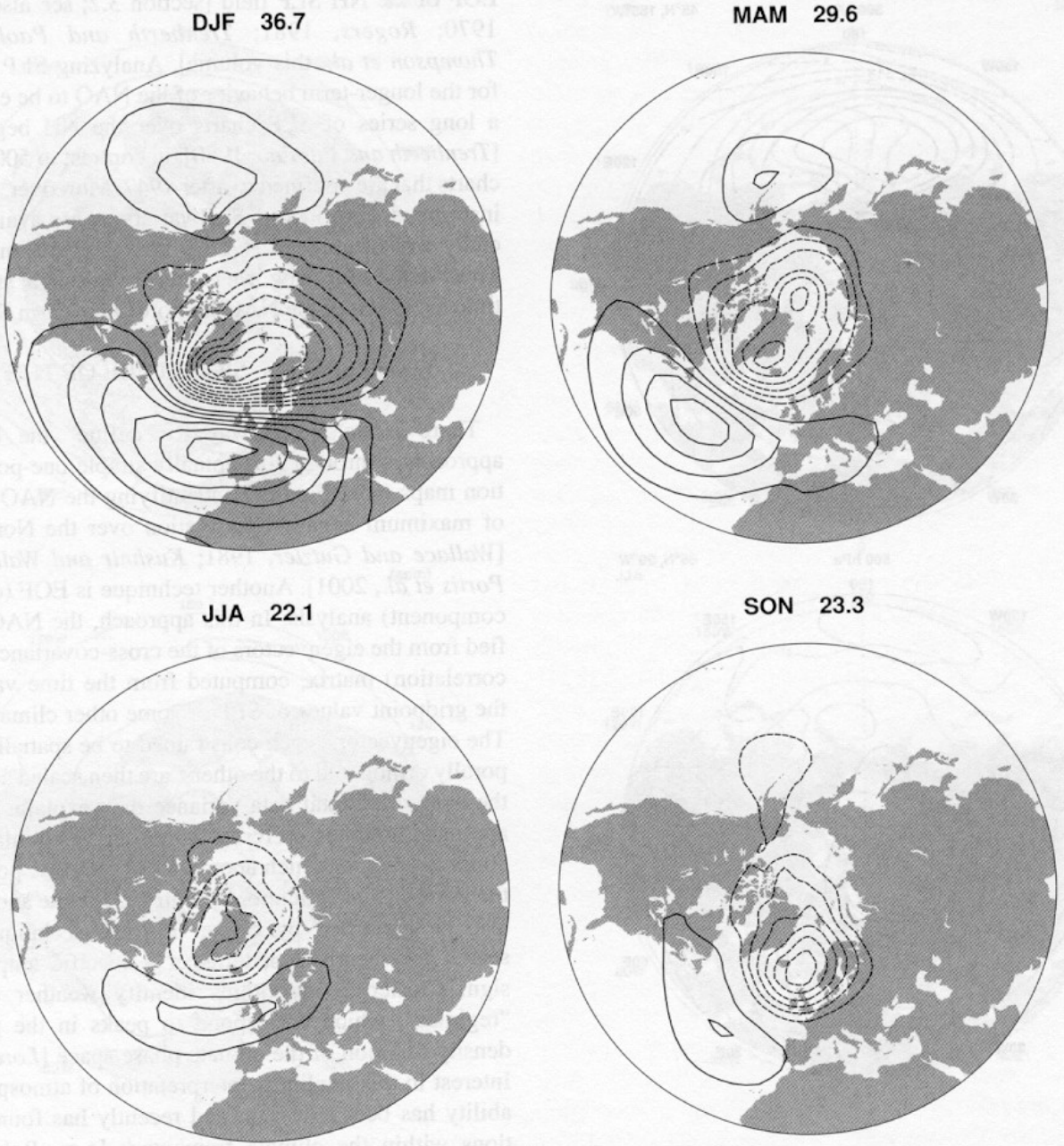

Figure 6. Leading empirical orthogonal functions (EOF 1) of the seasonal mean sea level pressure anomalies in the North Atlantic sector (20°-70°N, 90°W-40°E), and the percentage of the total variance they explain. The patterns are displayed in terms of amplitude (hPa), obtained by regressing the *hemispheric* sea level pressure anomalies upon the leading principal component time series. The contour increment is 0.5 hPa, and the zero contour has been excluded. The data cover 1899-2001 [see *Trenberth and Paolino,* 1980].

Hurrell et al. 2003

Changes in SLP and surface winds:

NAO positive: increased meridional pressure gradient and westerly winds.

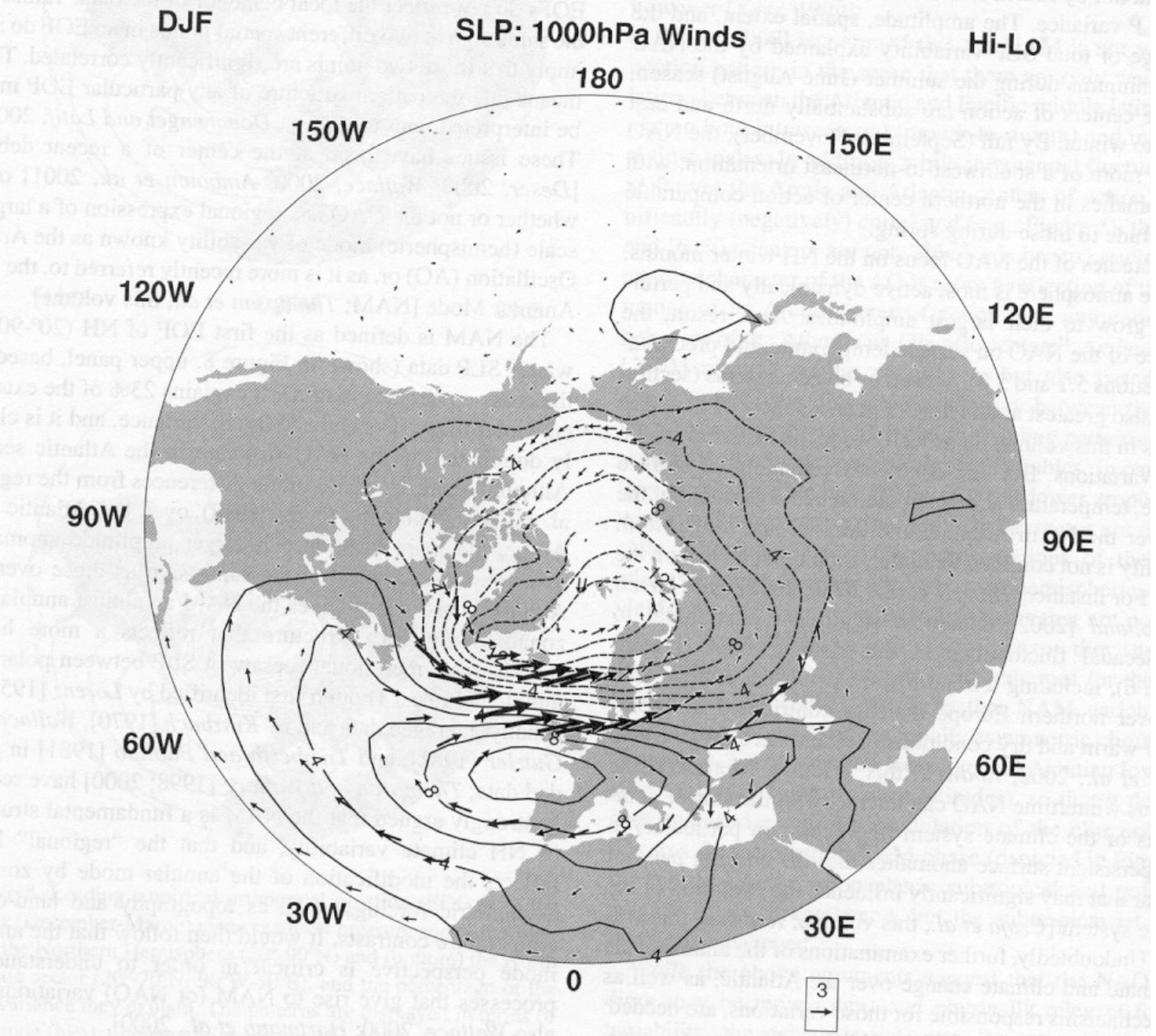

Figure 7. The difference in boreal winter (December-February) mean sea level pressure and 1000 hPa vector winds between positive (hi) and negative (lo) index phases of the NAO. The composites are constructed from winter data (the NCEP/NCAR reanalyses over 1958-2001) when the magnitude of the NAO index (defined as the principal component time series of the leading empirical orthogonal function of Atlantic-sector sea level pressure, as in Figures 6 and 10) exceeds one standard deviation. Nine winters are included in each composite. The contour increment for sea level pressure is 2 hPa, negative values are indicated by the dashed contours, and the zero contour has been excluded. The scaling vector is 3 m s^{-1}.

Hurrell et al. 2003

Marshall et al. 2001

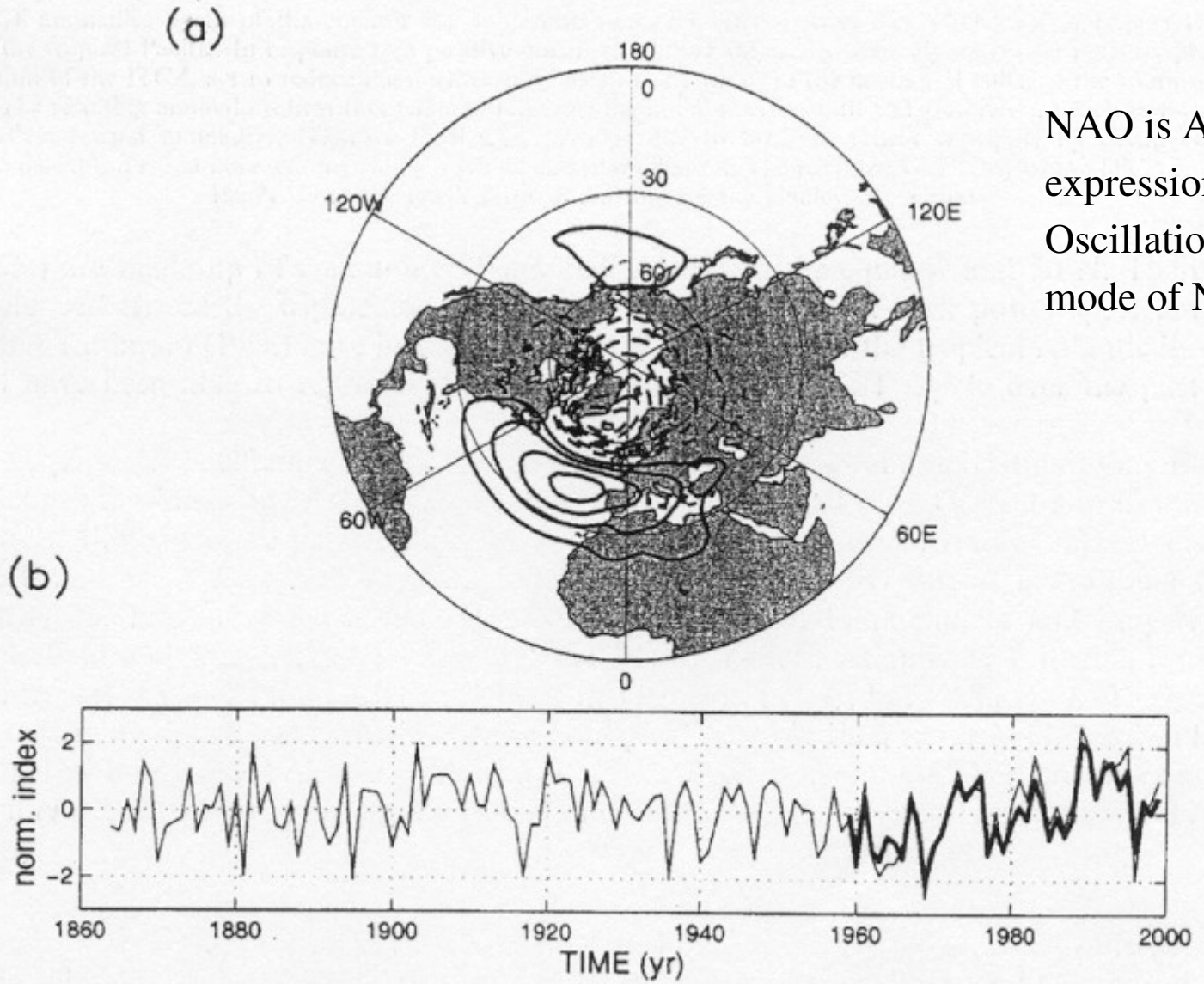

NAO is Atlantic expression of the Arctic Oscillation, the leading mode of NH SLP.

Figure 1. (a) Regression map of Northern Hemisphere SLP anomalies in winter (December–March 1958–1998) onto the first principal component of SLP anomalies over the North Atlantic sector (20°–70°N/100°W–20°E). (b) Time series of Hurrell's NAO index (thin curve) and the first principal component of SLP (thick curve). Both time series are normalized by their standard deviation. The SLP data are taken from the NCEP–NCAR reanalysis

Int. J. Climatol. **21**: 1863–1898 (2001)

Cluster analysis of SLP

Note the asymmetry

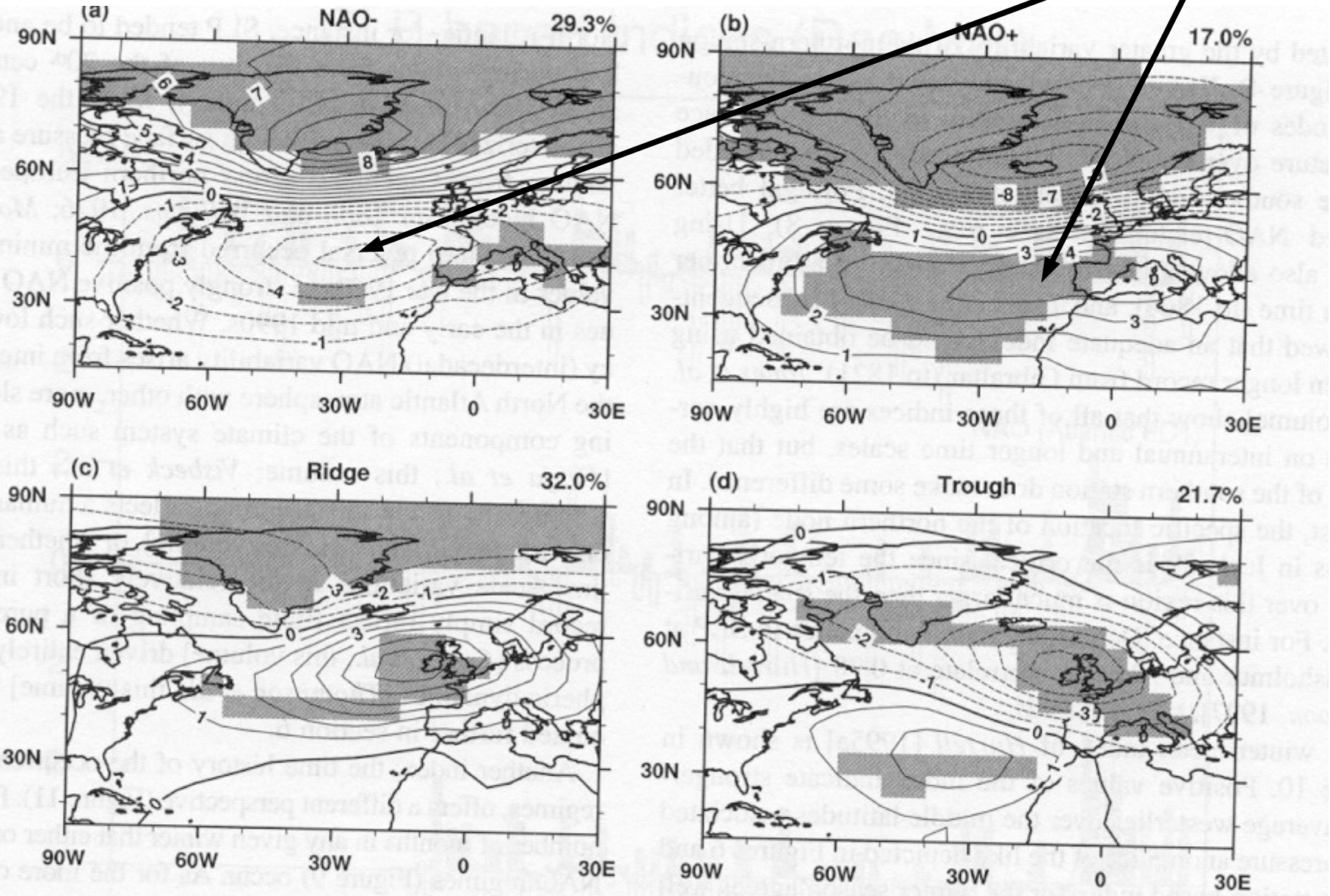

Figure 9. Boreal winter (December-March) climate regimes in sea level pressure (hPa) over the North Atlantic domain (20°-70°N, 90°W-40°E) using monthly data over 1900-2001. Shaded areas exceed the 95% confidence level using T and F statistics [see *Cassou*, 2001]. The percentage at the top right of each panel expresses the frequency of occurrence of a cluster out of all winter months since 1900. The contour interval is 1 hPa.

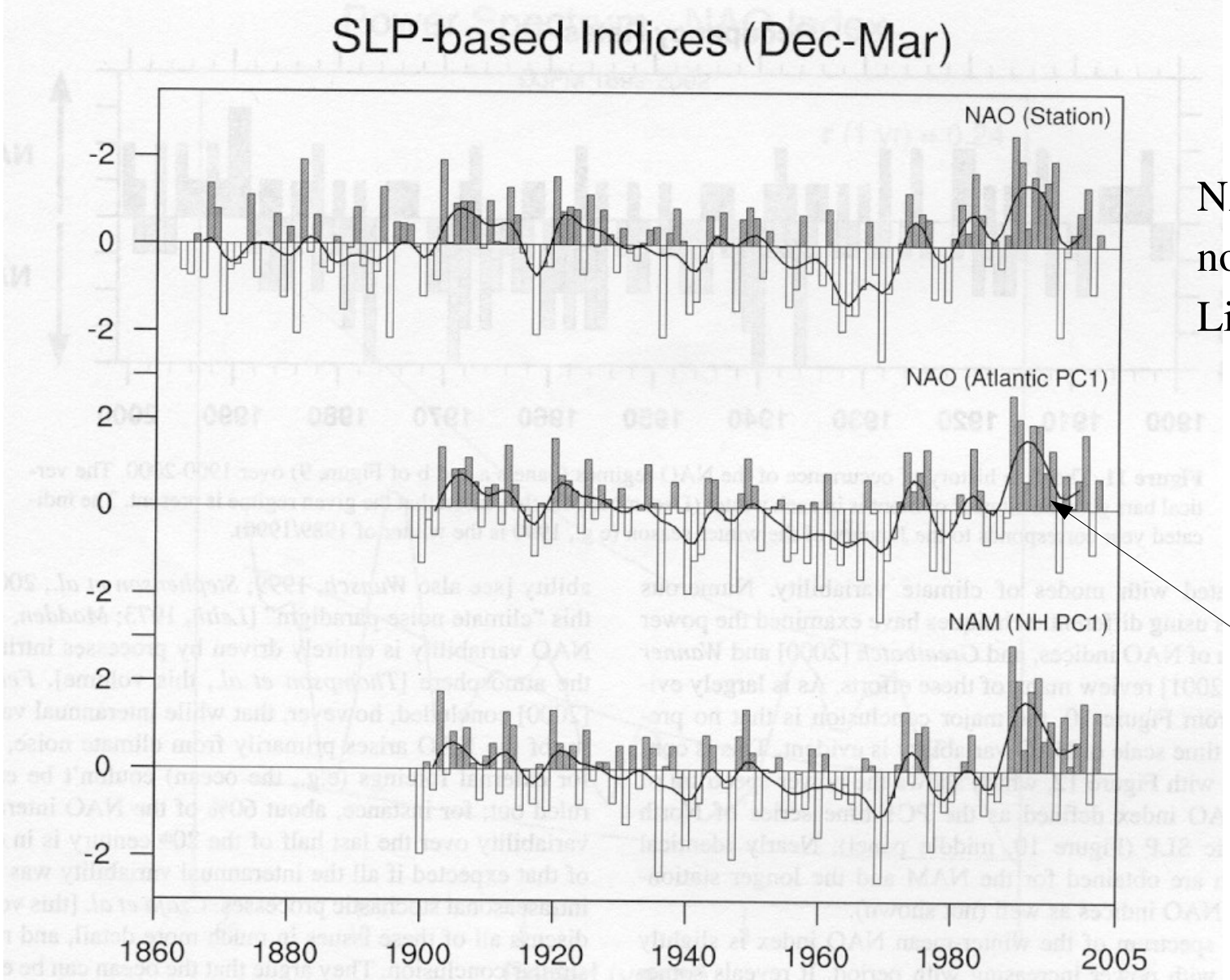

Figure 10. Normalized indices of the mean winter (December-March) NAO constructed from sea level pressure data. In the top panel, the index is based on the difference of normalized sea level pressure between Lisbon, Portugal and Stykkisholmur/Reykjavik, Iceland from 1864 through 2002. The average winter sea level pressure data at each station were normalized by division of each seasonal pressure by the long-term mean (1864-1983) standard deviation. In the middle panel, the index is the principal component time series of the leading empirical orthogonal function (EOF) of Atlantic-sector sea level pressure (bottom panel of Figure 8). In the lower panel, the index is the principal component time series of the leading EOF of Northern Hemisphere sea level pressure (top panel of Figure 8). The heavy solid lines represent the indices smoothed to remove fluctuations with periods less than 4 years. The indicated year corresponds to the January of the winter season (e.g., 1990 is the winter of 1989/1990). See http://www.cgd.ucar.edu/~jhurrell/nao.html for updated time series.

NAO index: difference of normalized SLP between Lisbon and Reykjavik

Persistent positive perturbations

Cluster analysis: 'time series'

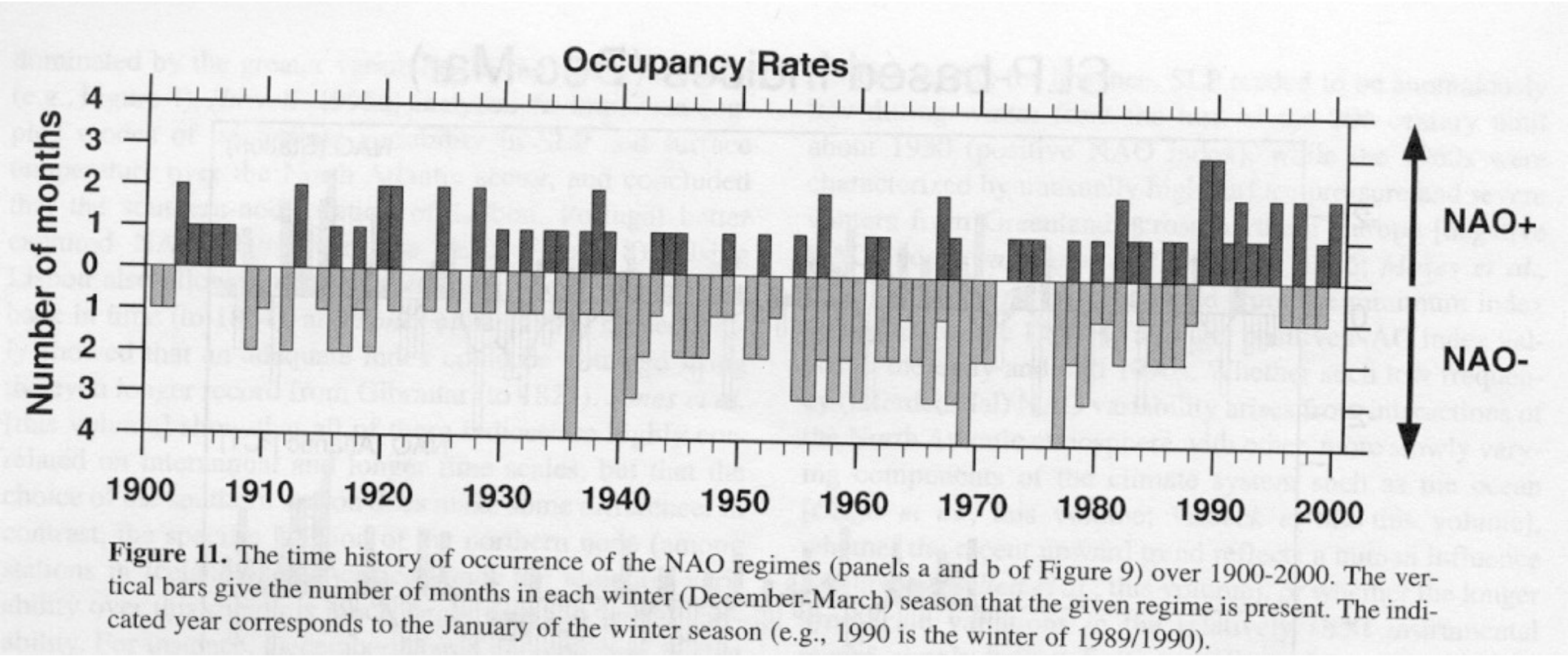

Figure 11. The time history of occurrence of the NAO regimes (panels a and b of Figure 9) over 1900-2000. The vertical bars give the number of months in each winter (December-March) season that the given regime is present. The indicated year corresponds to the January of the winter season (e.g., 1990 is the winter of 1989/1990).

Note the strong interannual variation of the regime occurrence, e.g. 1960s dominated by NAO- and 1990s by NAO+

Also note the large within season variations, with both regimes occupied during a single winter.

Low frequency variability/trend

1981-2002 minus 1951-1980 averages.

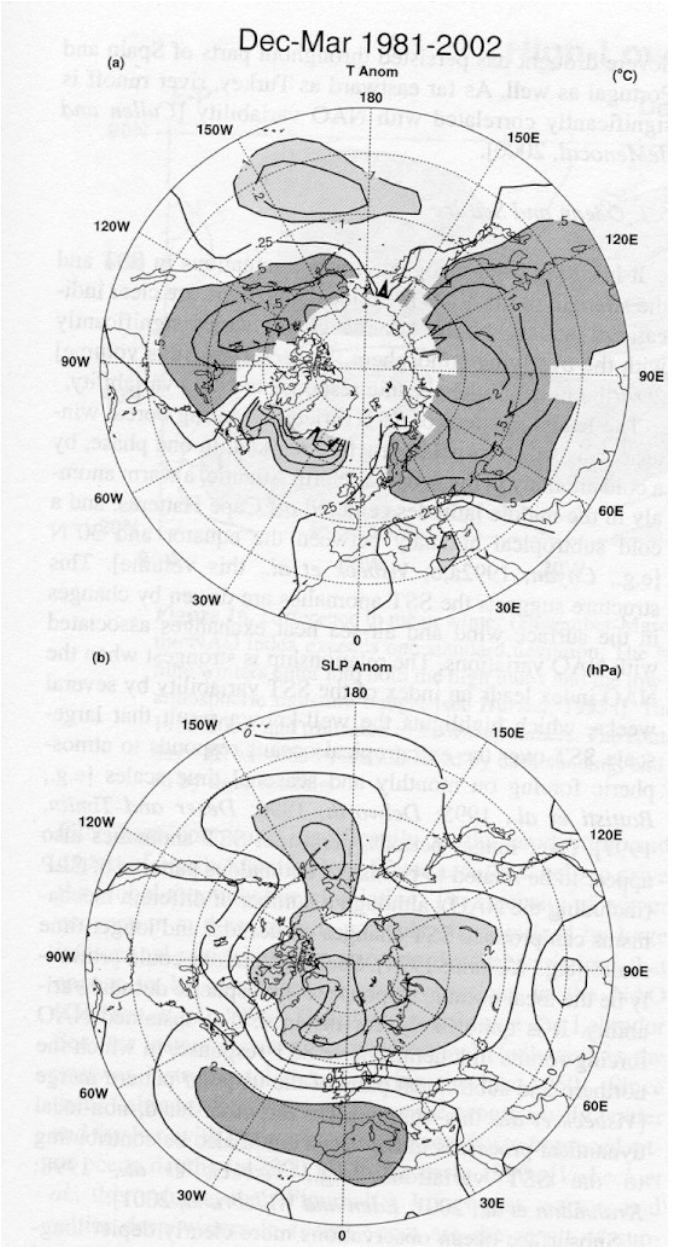

Figure 14. Twenty-two (1981-2002) winter (December-March) average (a) land surface and sea surface temperature anomalies and (b) sea level pressure anomalies expressed as departures from the 1951-1980 means. Temperature anomalies > 0.25°C are indicated by dark shading, and those < -0.10°C are indicated by light shading. The contour increment is 0.1°C for negative anomalies, and the 0.25, 0.5, 1.0, 1.5, and 2.0°C contours are plotted for positive anomalies. Regions with insufficient temperature data are not contoured. The same shading convention is used for sea level pressure, but for anomalies greater than 2 hPa in magnitude. The contour increment in (b) is 1 hPa.

Temperature

Surface pressure

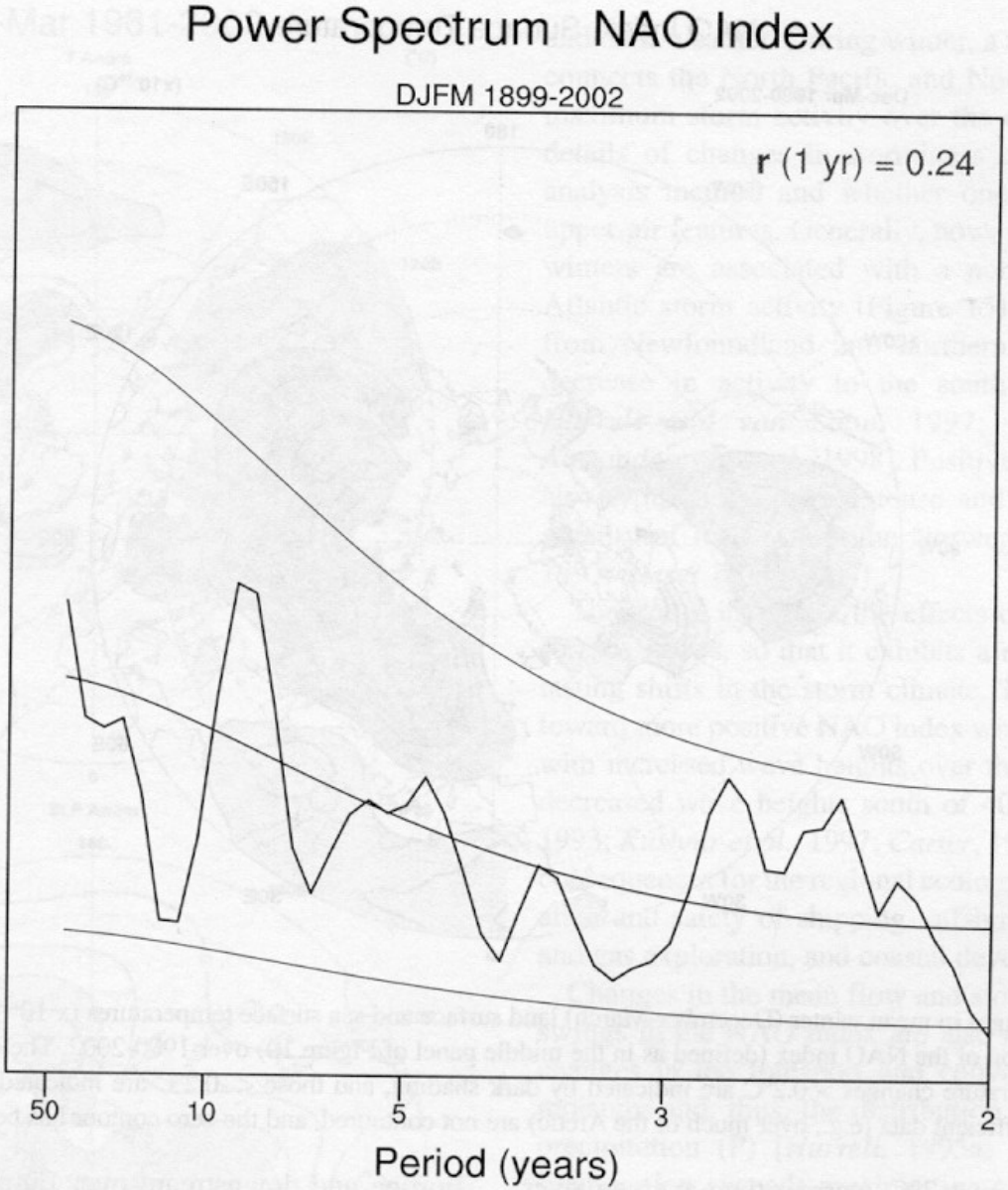

Figure 12. Power spectrum of the mean winter (December-March) NAO index over 1899-2002, defined as in the middle panel of Figure 10. Also shown is the corresponding red noise spectrum with the same lag one autocorrelation coefficient (0.24) and the 5 and 95% confidence limits.

Slightly red spectrum

NAO impacts

Impact of NAO on storm tracks

Northward shift of storm track

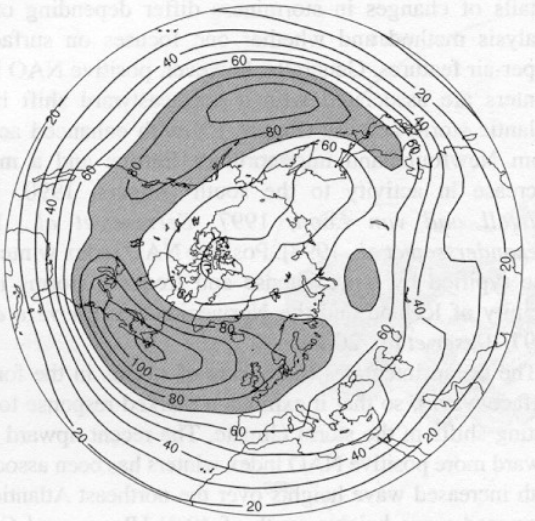

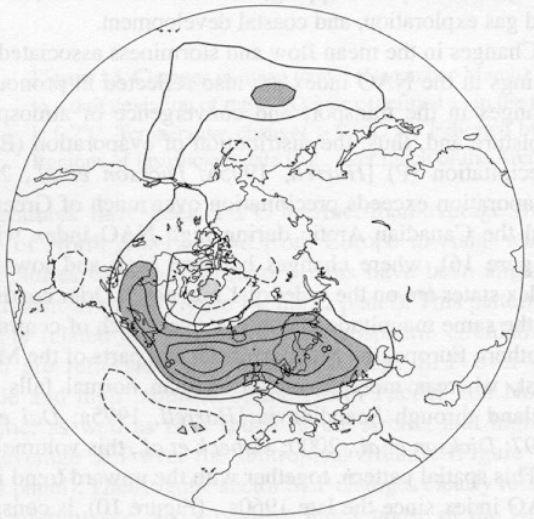

Figure 15. In the top panel, mean storm tracks for 1958-1998 winters (December-March) as revealed by the 300 hPa root mean square transient geopotential height (gpm) bandpassed to include 2-8 day period fluctuations. Values greater than 70 gpm are shaded and the contour increment is 10 gpm. In the lower panel, anomalies are expressed in terms of amplitude (gpm) by regression onto the NAO index (defined as in the middle panel of Figure 10). The contour increment is 2 gpm, and anomalies greater than 4 gpm in magnitude are shaded. The data come from the NCEP/NCAR reanalyses.

Impact on fresh water flux, E-P

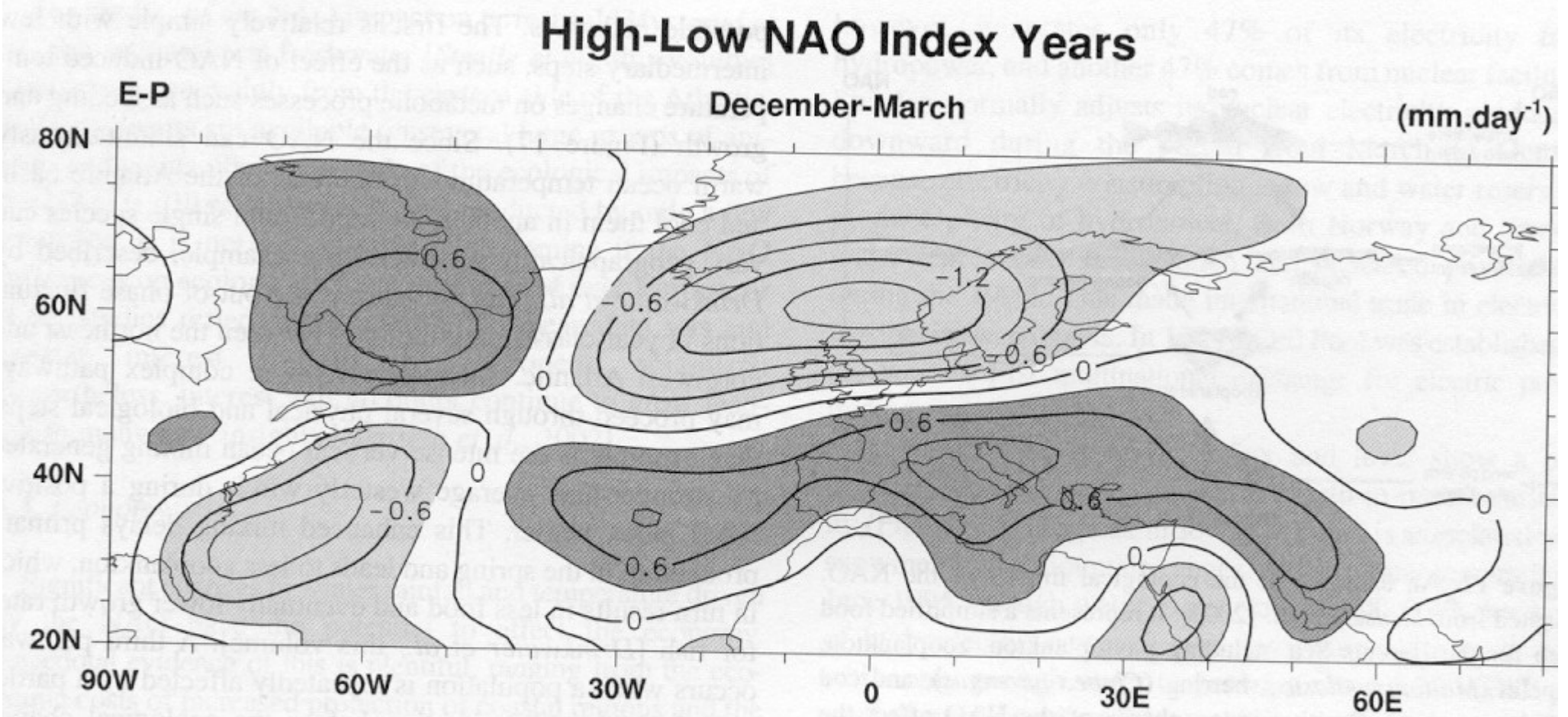

Figure 16. Difference in mean winter (December-March) evaporation (E) minus precipitation (P) between years when the NAO index exceeds one standard deviation. The NAO index is defined as in the middle panel of Figure 10, and nine winters enter into both the high index and the low index composites. The E-P field is obtained as a residual of the atmospheric moisture budget [see *Hurrell*, 1995a]. The calculation was based on the NCEP/NCAR reanalyses over 1958-2001, and truncated to 21 wavenumbers. The contour increment is 0.3 mm day^{-1}, differences greater than 0.3 mm day^{-1} (E exceeds P) are indicated by dark shading, and differences less than -0.3 mm day^{-1} (P exceeds E) are indicated by light shading.

Impact on surface temperature

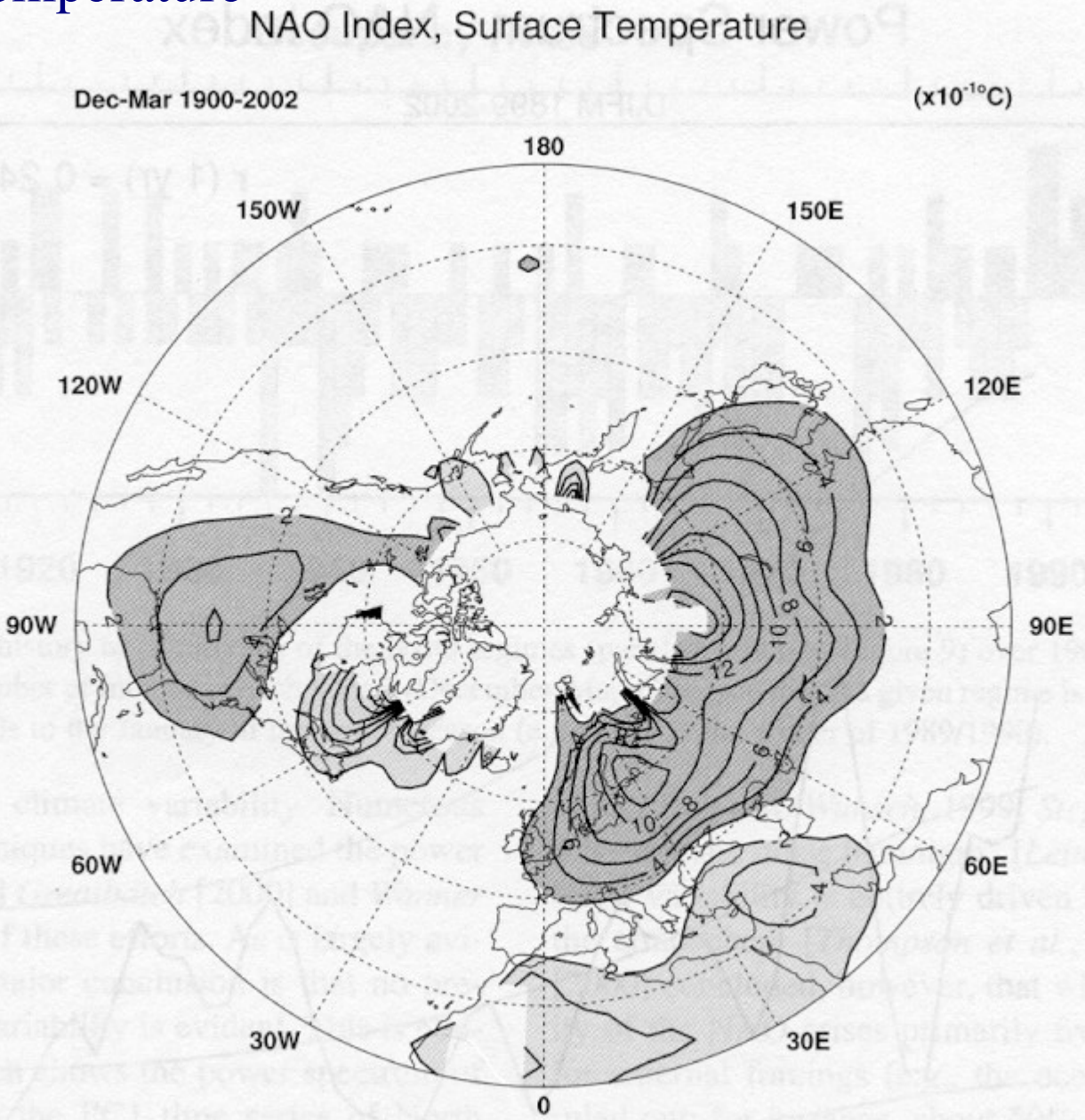

Figure 13. Changes in mean winter (December-March) land surface and sea surface temperatures (x 10^{-1}°C) corresponding to a unit deviation of the NAO index (defined as in the middle panel of Figure 10) over 1900-2002. The contour increment is 0.2°C. Temperature changes > 0.2°C are indicated by dark shading, and those < -0.2°C are indicated by light shading. Regions of insufficient data (e.g., over much of the Arctic) are not contoured, and the zero contour has been excluded.

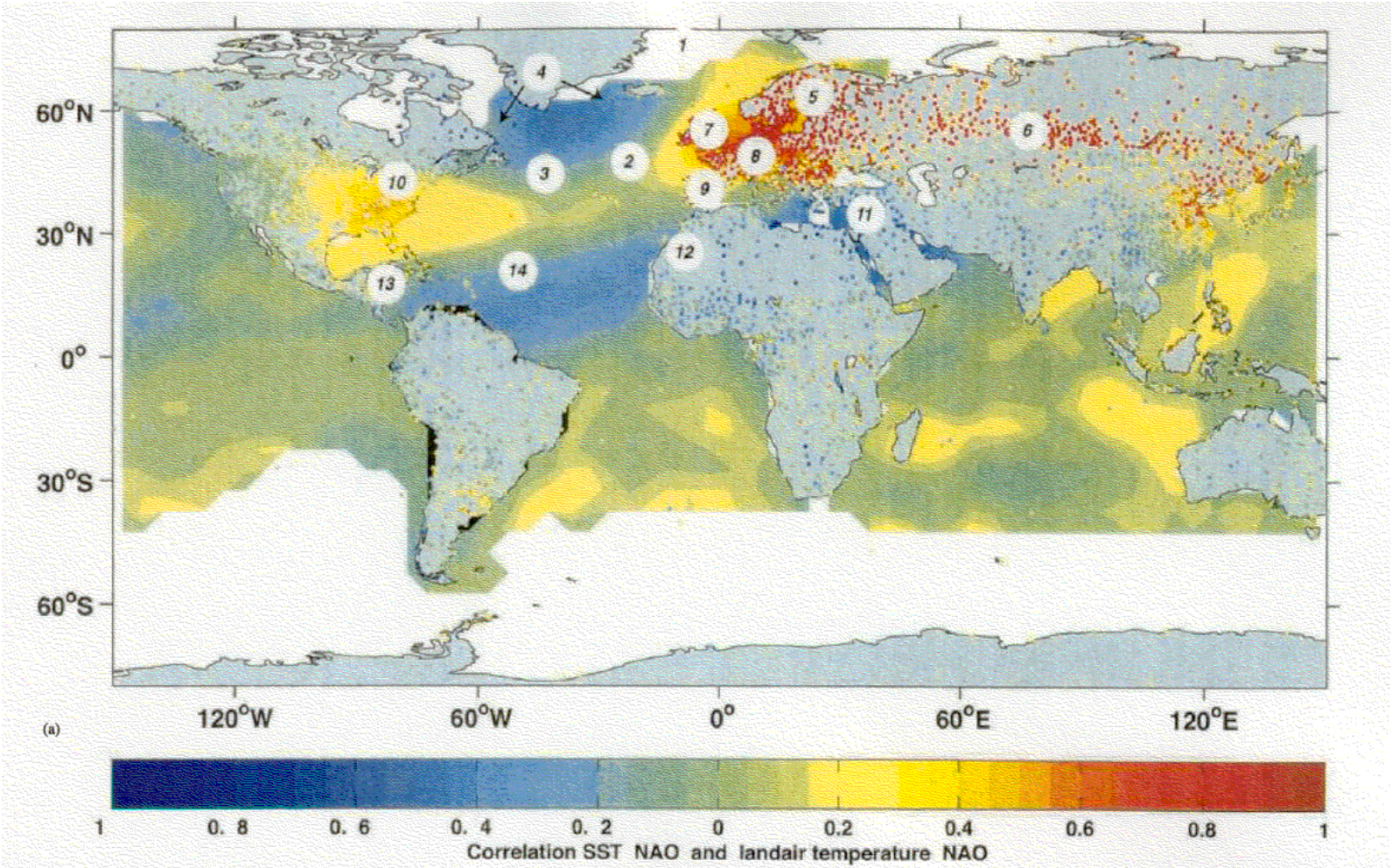

Plate 1. Impacts of Atlantic climate variability. (a) shows the correlation between the December–March NAO index (Hurrell, 1995b) and global surface temperature. SST is used over the oceans, and station air temperature over land. SST is taken from Kaplan *et al.* (1998) and station data are from NOAA/NCDA/GHCN (Vose *et al.*, 1992; Peterson and Vose, 1997). Numbers in grey circles refer to the entries in Table I (see left column). (b) shows the correlation between an index of the tropical Atlantic cross equatorial SST gradient (also known as the TDI, see Chang *et al.*, 1997) and rainfall (over land) and SST (over the oceans). SST data are taken from Kaplan *et al.* (1998) and rainfall from NOAA/NCDC/GHCN station data. All anomalies are annual (i.e. calculated from the difference between annual averages derived from monthly data and the long-term annual mean climatology)

Table I. NAO-related climatic impacts that have been discussed in the literature. The first column provides a cross-reference number with Panel A of Plate 1. Other columns indicate the region of influence, the climatic variables affected and literature references, respectively. The reference list is representative but not exhaustive

No.*	Region of Influence	Phenomena	References
1	Arctic	Winter temperature, precipitation, sea ice distribution and movement.	Walsh and Johnson (1979); Kelly *et al.* (1982); Appenzeler *et al.* (1998); Kwok and Rothrock (1999); Parkinson *et al.* (1999).
2	North Atlantic	Winter storminess and ocean wave heights.	Dickson and Namias (1976); Carter and Draper (1988); Bacon and Carter (1991, 1993); Rogers (1997); Kushnir *et al.* (1997); The WASA Group (1998).
3	North Atlantic	Marine ecosystems, fisheries.	Dickson and Brander (1993); Post *et al.* (1997); Fromentin and Planque (1996); Dippner (1997); Fromentin *et al.* (1998); Reid *et al.* (1998); Planque and Taylor (1998); Marsh *et al.* (1999); Belgrano *et al.* (1999); Weyhenmeyer *et al.* (1999).
4	North Atlantic marginal seas	Atlantic sea ice anomalies.	Kelly *et al.* (1987); Walsh and Johnson (1979); Deser and Balckmon (1993); Deser *et al.* (2000).
5	Northwest Europe; Scandinavia	Winter temperature, rainfall and the severity of winters/effects on wildlife and plants.	Petterssen (1949); van Loon and Rogers (1978); Rogers (1985); Hurrell (1995b); Hurrell and van Loon (1997b); Thompson and Wallace (1998); Forchhammer *et al.* (1998); Loewe and Koslowski (1998); Wibig (1999); Chen and Hellstrom (1999); Post *et al.* (1999a,b); Post and Stenseth (1999).
6	Northeast Asia; Siberia	Winter temperature and rainfall.	Peng and Mysak (1993); Hurrell (1995b); Hurrell and van Loon (1997); Thompson and Wallace (1998); Livingstone (1999b).
7	British Isles	Rainfall, temperature and their ecological effects.	Rogers and van Loon (1979); Hurrell and van Loon (1997) Wibig (1999); Benner (1999); Kiely (1999); Milner *et al.* (1999); Colman and Davey (1999).
8	Central Europe	Winter temperature.	Walker and Bliss (1932); van Loon and Rogers (1978).
9	Southwestern Europe	Rainfall.	Rogers and van Loon (1979); Hurrell and van Loon (1997); Rodo *et al.* (1997); Ulbrich and Christoph (1999).
10	North America (Labrador, Hudson Bay, central US)	Winter temperature and snowfall/ effect on wildlife.	Hurrell (1995b); Hurrell (1996); Hartley and Keables (1998); Hartley, 1999; Post and Stenseth (1998); Post *et al.* (1999); Stenseth *et al.* (1999).
11	Mediterranean and the Middle East	Winter rainfall, temperature.	Metaxas *et al.* (1991); Kutiel and Kay, 1992; Cullen and de Menocal (2000).
12	North Africa—Morocco	Winter rainfall.	Lamb and Peppler (1987).
13	Central America, Caribbean	Rainfall.	Giannini *et al.* (2000).
14	Tropical North Atlantic (through SST)	Hurricane occurrence and tracks.	Landsea *et al.* (1999); Shapiro and Goldenberg (1998).

* The numbers in this column refer to those in the grey circles that appear in Plate 1.

NAO: a mode of internal atmospheric variability

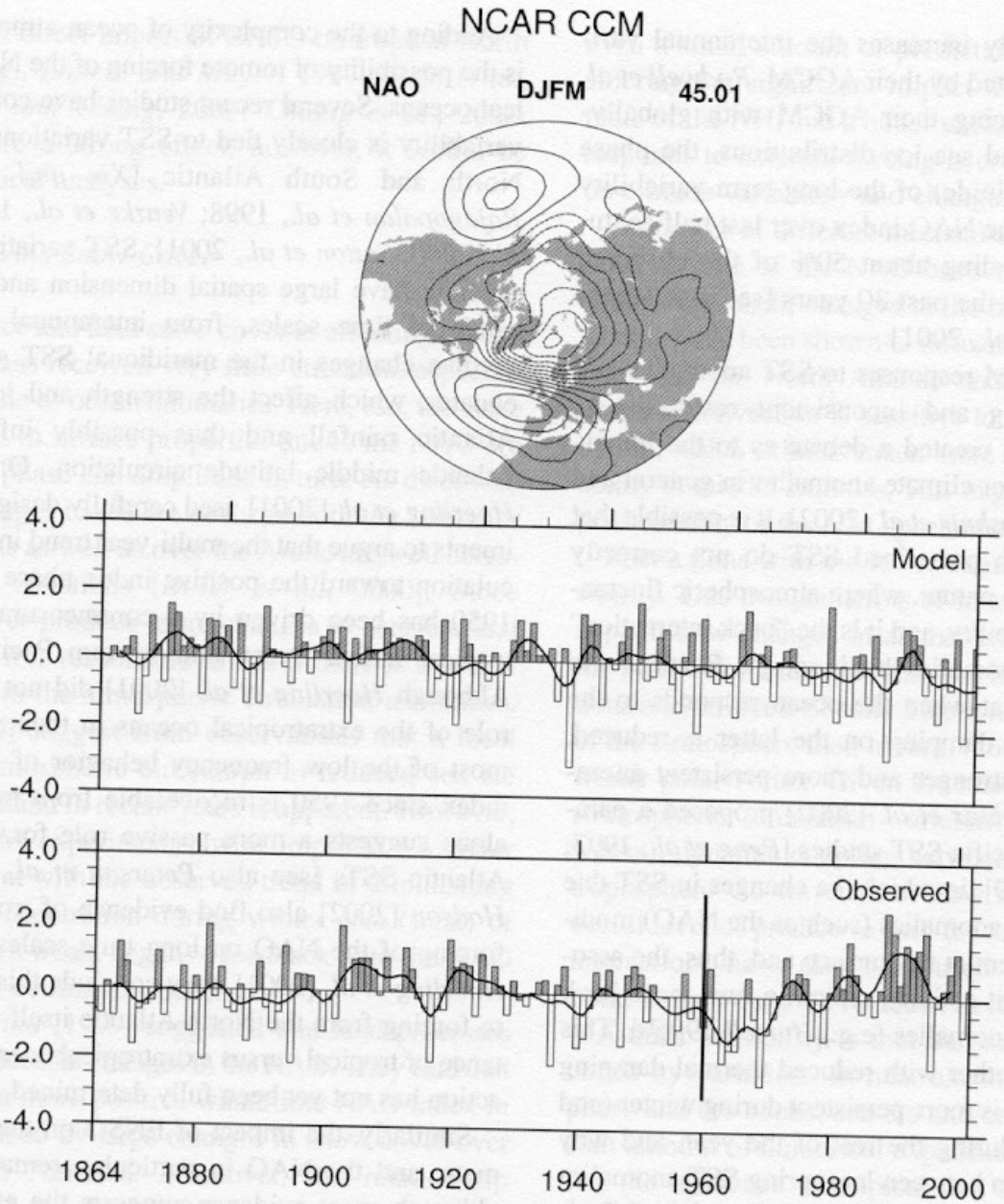

Figure 19. Leading empirical orthogonal function (EOF 1) of the winter (December-March) mean sea level pressure anomalies over (top) the North Atlantic sector (20°-70°N, 90°W-40°E), and the percentage of the total variance it explains in a 200 year integration with the NCAR Community Climate Model (CCM) with climatological annual cycles of all forcings external to the atmosphere. The pattern is displayed in terms of amplitude (hPa), obtained by regressing the hemispheric sea level pressure anomalies upon the leading principal component time series. A subset of 139 years of the latter is plotted in the middle panel for comparison to the station-based NAO index (lower panel) of equivalent length (upper panel of Figure 10). Both the model and observed NAO indices have been normalized. In the top panel, the contour increment is 0.5 hPa, and the zero contour has been excluded.

Atlantic or hemispheric phenomena?

NAO or AO (Arctic Oscillation)

Leading EOF of sea level pressure in northern hemisphere (top) and in Atlantic sector are similar, but differ in Pacific sector.

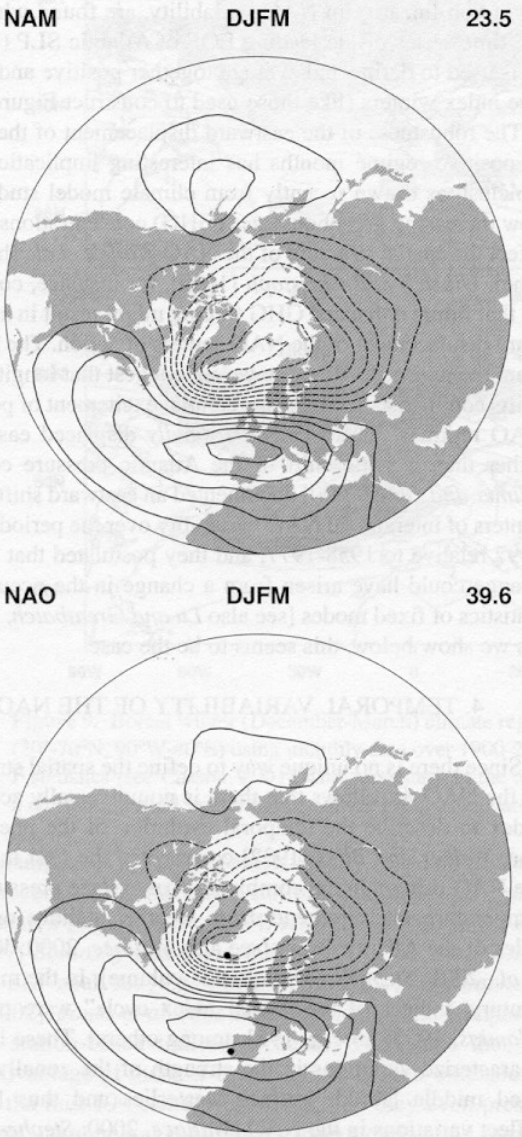

Figure 8. Leading empirical orthogonal function (EOF 1) of the winter (December-March) mean sea level pressure anomalies over (top) the Northern Hemisphere (20°-90°N) and (bottom) the North Atlantic sector (20°-70°N, 90°W-40°E), and the percentage of the total variance they explain. The patterns are displayed in terms of amplitude (hPa), obtained by regressing the *hemispheric* sea level pressure anomalies upon the leading principal component time series. The contour increment is 0.5 hPa, and the zero contour has been excluded. The data cover 1899-2001 [see *Trenberth and Paolino,* 1980]. The dots in the bottom panel represent the locations of Lisbon, Portugal and Stykkisholmur, Iceland used in the station based NAO index of *Hurrell* [1995a] (see Figure 10).

Similarity of northern and southern hemisphere annular modes

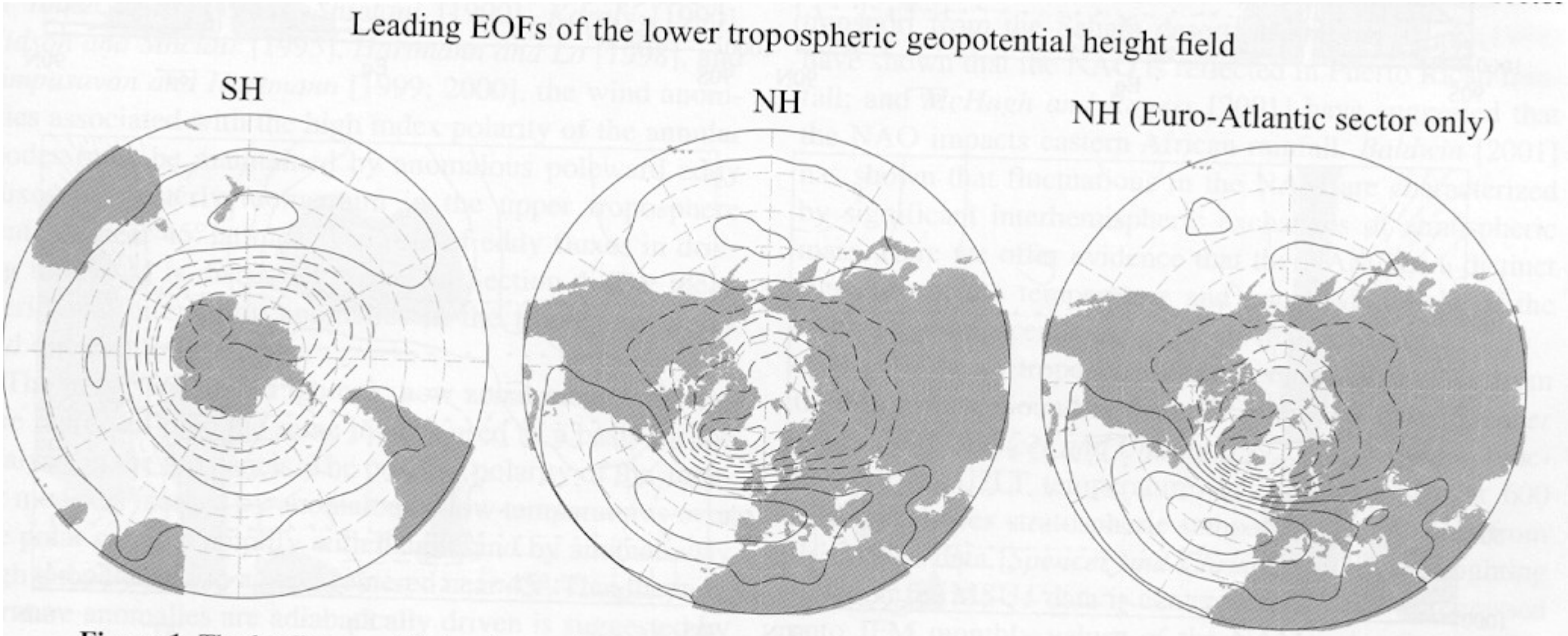

Figure 1. The leading empirical orthogonal function (EOF 1) of the Southern Hemisphere (SH; 90°S-20°S) monthly-mean 850-hPa height field (*left panel*); the Northern Hemisphere (NH; 20°N-90°N) monthly-mean SLP field (*middle panel*); and the monthly-mean SLP field in the Euro-Atlantic sector (20°N-90°N, 60°W- 30°E) (*right panel*). The pattern in the right panel has been extended to include the entire hemisphere by regressing the monthly-mean SLP field upon the corresponding principal component time series. SLP is displayed in units of geopotential height at 1000-hPa. Contour interval 10 m (-5, 5, 15...); negative contours are dashed. Results are based on monthly-mean fields of the NCEP/NCAR Reanalyses (January-March for the NH; all months for the SH) for the period 1958-99. Figures duplicated from *Thompson and Wallace* [2000] and *Wallace and Thompson* [2002].

Equivalent barotopic largest in stratosphere

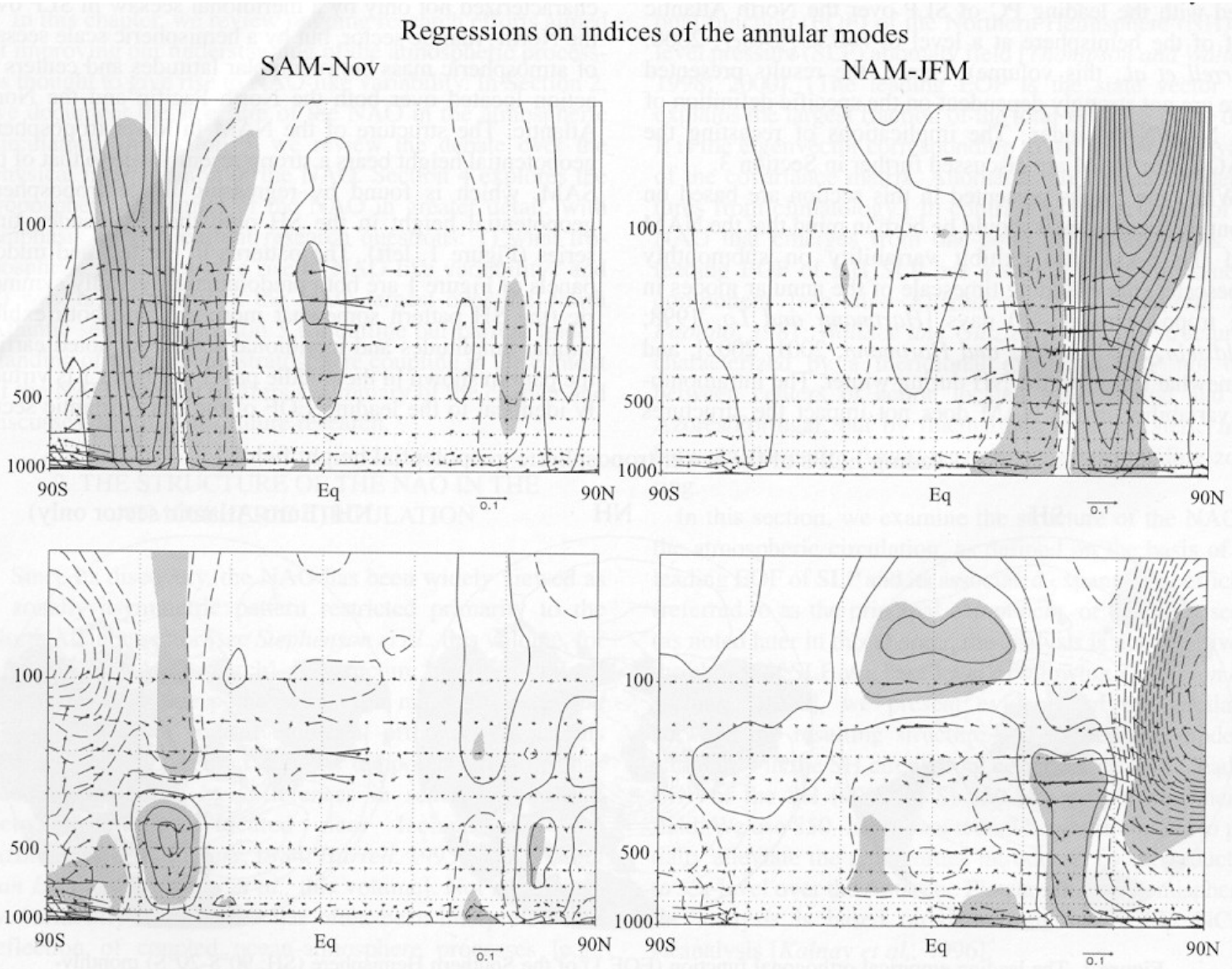

Figure 2. Top: Zonal-mean zonal flow (contours) and mean meridional circulation (vectors) regressed onto the standardized monthly time series of the annular modes for the "active seasons" of stratosphere/troposphere coupling based on monthly data, January-March (NH) and November (SH), from 1979-1999. Bottom: As in the top panel but contours are for zonal-mean temperature. Contour intervals are 0.5 m s^{-1} (-0.75, -0.25, 0.25) for zonal wind and 0.2 K (-0.3, -0.1, 0.1) for temperature. Vectors are in units of m s^{-1} for the meridional wind component; cm s^{-1} for the vertical component (scale at bottom). Shading indicates correlations of $r > 0.4$. The top of the diagram corresponds to 50-hPa. Figure adapted from *Thompson and Wallace* [2000].

Stratosphere: time scale of several weeks

Troposphere/NAO: time scale of about 10 days

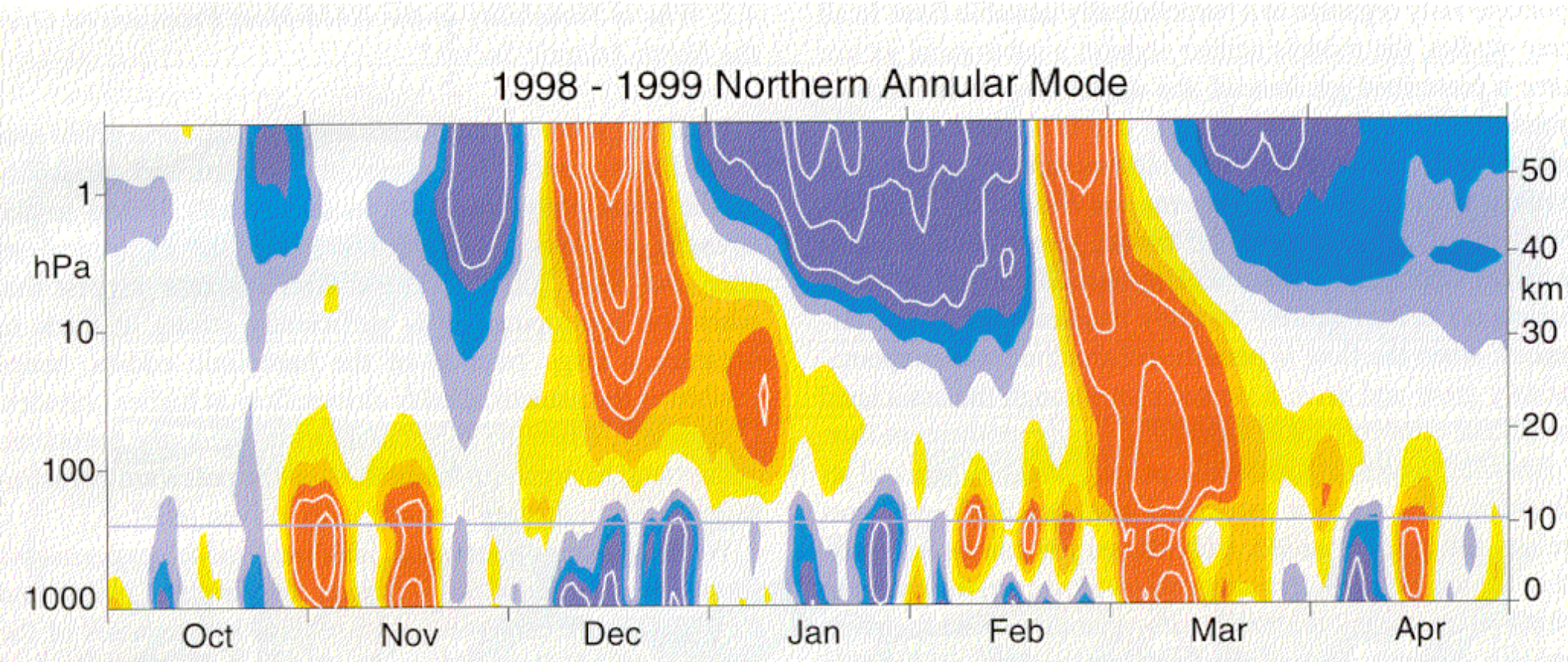

Plate 2. Time-height development of the NAM during the winter of 1998–1999. The indices have daily resolution and are nondimensional. Blue corresponds to positive values (strong polar vortex) and red corresponds to negative values (weak polar vortex). The contour interval is 0.5, with values between -0.5 and 0.5 unshaded. The thin horizontal line indicates the approximate boundary between the troposphere and the stratosphere. From *Baldwin and Dunkerton* [2002].

Coupling of stratosphere and troposphere

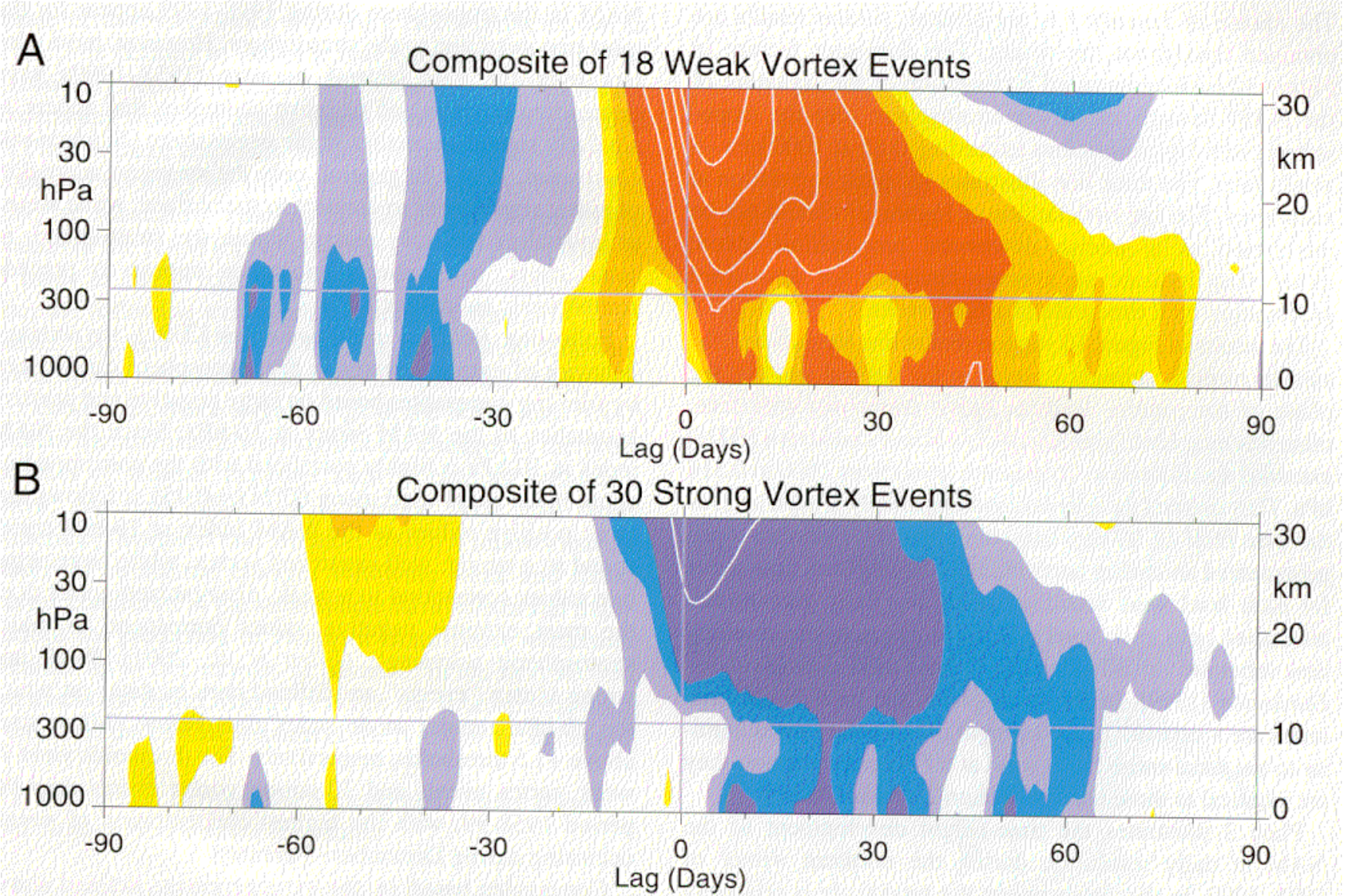

Plate 4. Composites of the time-height development of the NAM for (a) 18 weak vortex events and (b) 30 strong vortex events. The events are determined by the dates on which the NAM at 10-hPa crosses –3.0 and +1.5, respectively. The indices are nondimensional; the contour interval for the color shading is 0.25, and 0.5 for the white contours. Values between -0.25 and 0.25 are unshaded. The thin horizontal lines indicate the approximate boundary between the troposphere and the stratosphere. From *Baldwin and Dunkerton* [2002].

Average daily sea level pressure associated with strong polar vortex

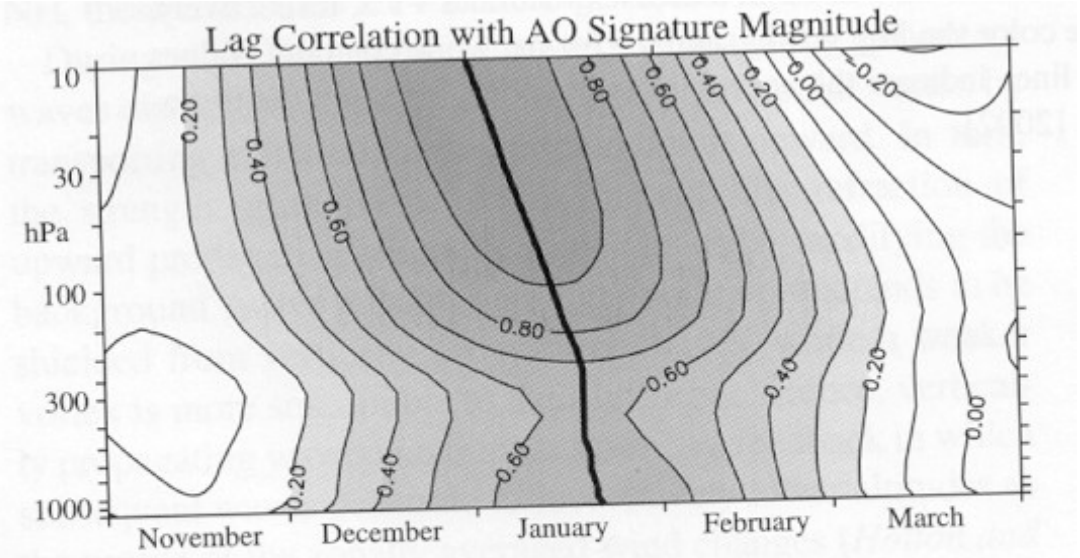

Figure 10. Correlations between the 90-day low-pass annular mode values at 10 hPa on January 1 with the annular mode values at all levels during November-March. From *Baldwin and Dunkerton* [1999].

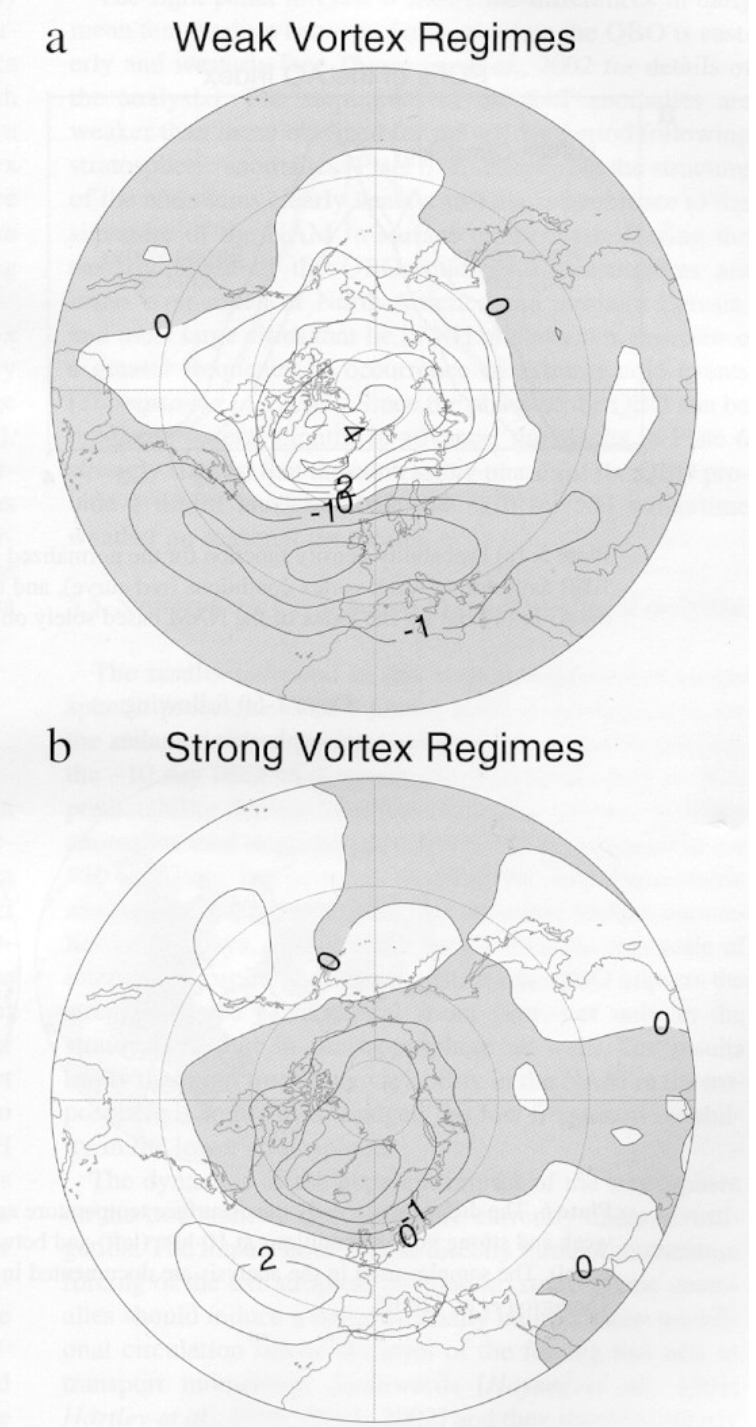

Figure 11. Average sea level pressure anomalies (hPa) for (a) the 1080 days during weak vortex conditions and (b) the 1800 days during strong vortex conditions. From *Baldwin and Dunkerton* [2002].

NAO and global warming

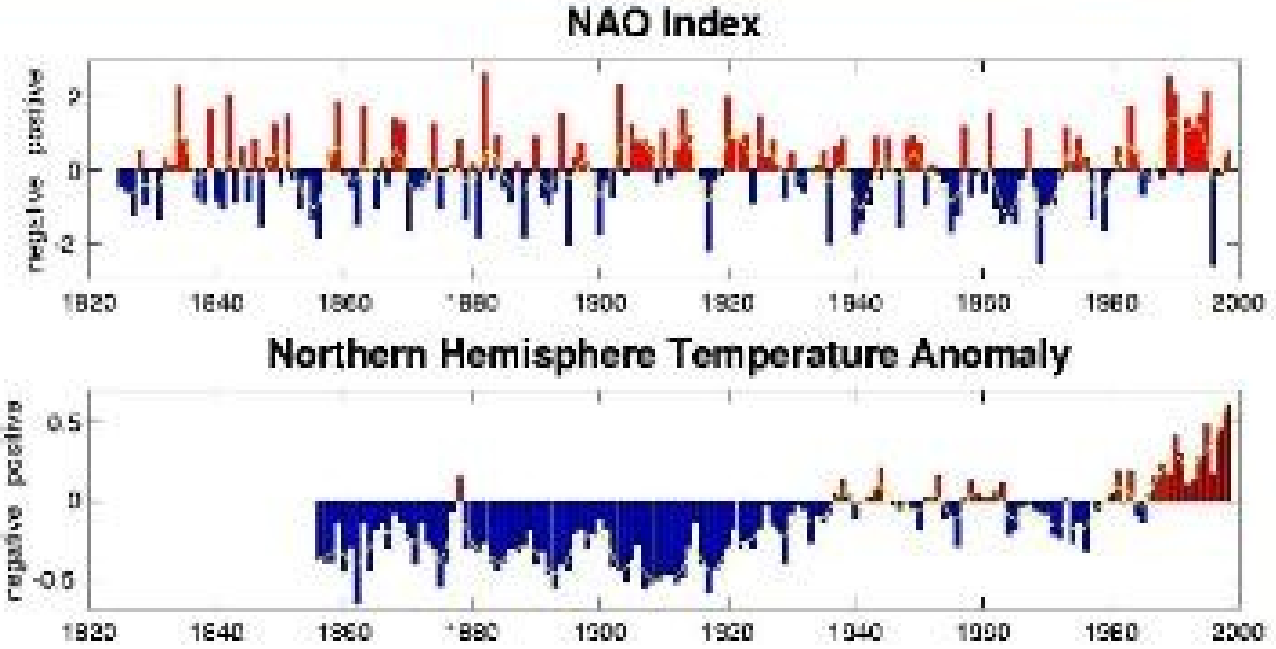

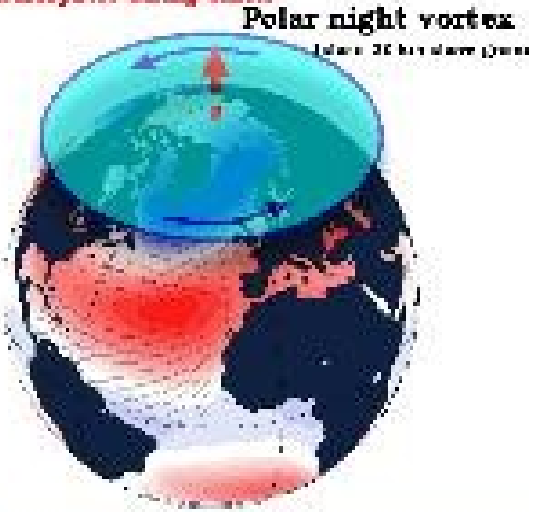

- Some scientist argue that changes in the stratospheric circulation can influence the phase of the NAO.
- Ozone depletion and increase of CO2 both result in a strong polar night vortex which might cause the NAO to prefer a positive state.
- Will "global warming" cause a persistent positive NAO phaes?

Martin Ticback Feb 04, 2000

Ocean Response

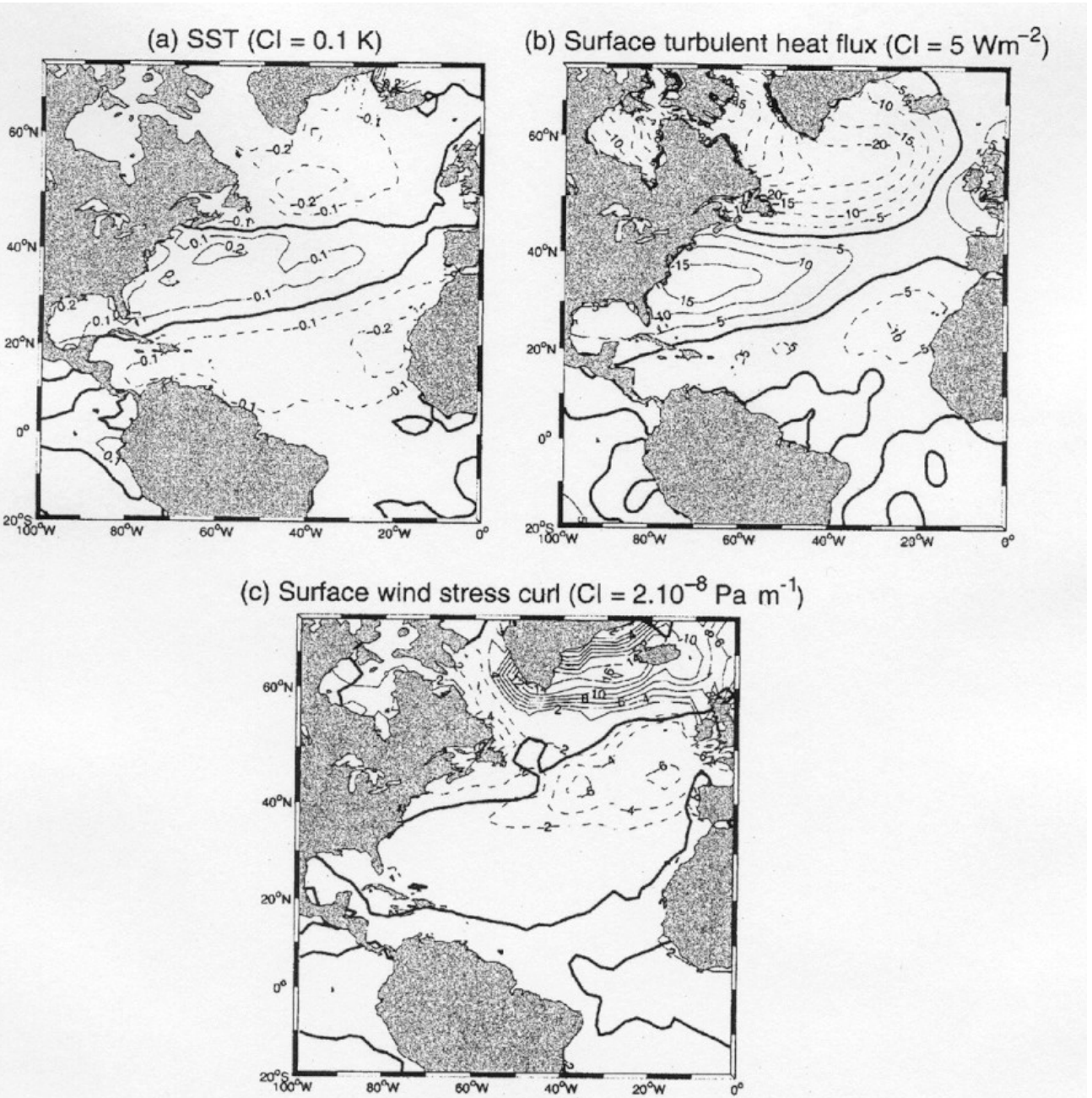

Figure 2. Regression maps of (a) SST (CI = 0.1 K, negative dashed), (b) surface turbulent heat flux (latent + sensible, CI = 5 Wm^{-2}, dashed out of the ocean) and (c) surface wind stress curl (CI = 2×10^{-3} Pa m^{-1}, dashed for anticyclonic) anomalies onto the NAO index shown in Figure 1(b). The thick black line is the zero wind curl line of the climatological winds. The SST and wind stress curl data come from the NCEP–NCAR reanalysis, while the surface heat flux anomalies come from Da Silva *et al.* (1994). A linear trend was removed to all datasets prior to computing the linear regressions

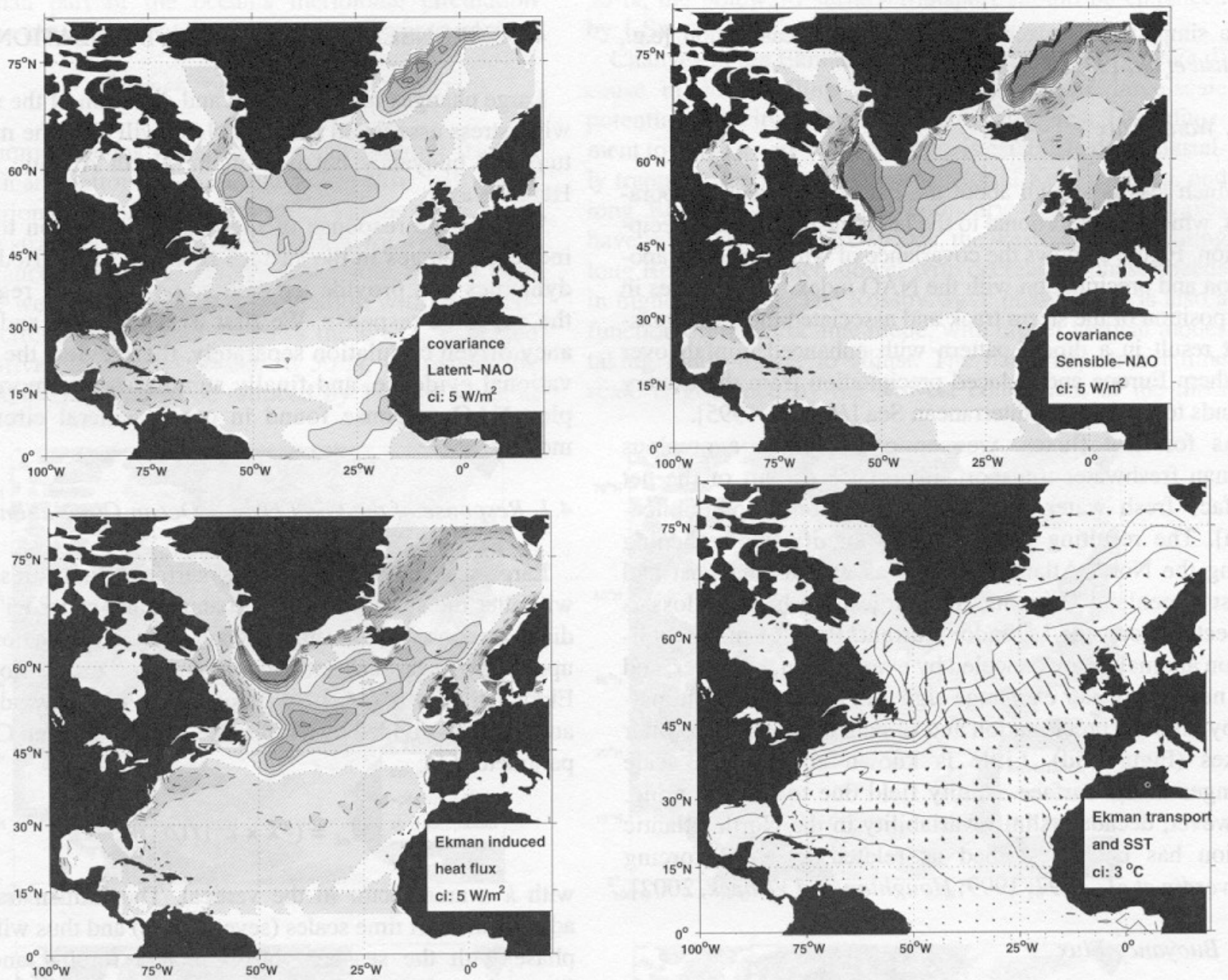

Figure 4. The graph shows the covariance between the NAO-index and the NCEP/NCAR reanalysis (1958–2000) latent heat flux (top left) and the sensible heat flux (top right). Changes in the Ekman transport (bottom right) alter the upper ocean heat transport and its divergence is expressed as a surface heat flux (bottom left). The solid lines in the lower right graph show the climatological winter SSTs and the arrows represent the NAO-induced surface Ekman transport.

SST anomalies persist, consistent with reemergence, correlation of NAO with SST leading might indicate an active ocean to atmosphere feedback

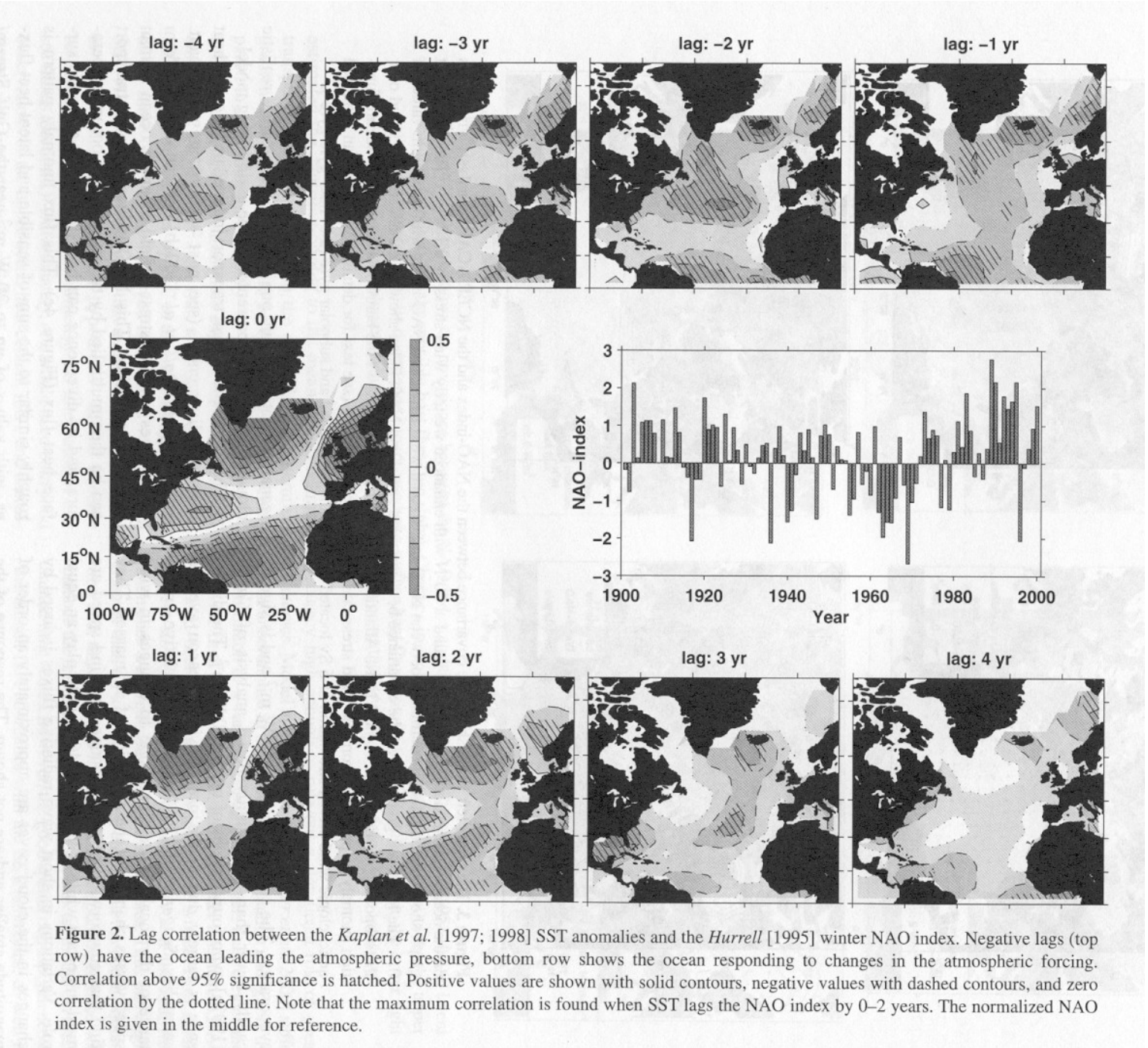

Figure 2. Lag correlation between the *Kaplan et al.* [1997; 1998] SST anomalies and the *Hurrell* [1995] winter NAO index. Negative lags (top row) have the ocean leading the atmospheric pressure, bottom row shows the ocean responding to changes in the atmospheric forcing. Correlation above 95% significance is hatched. Positive values are shown with solid contours, negative values with dashed contours, and zero correlation by the dotted line. Note that the maximum correlation is found when SST lags the NAO index by 0–2 years. The normalized NAO index is given in the middle for reference.

Advection of SST anomalies?

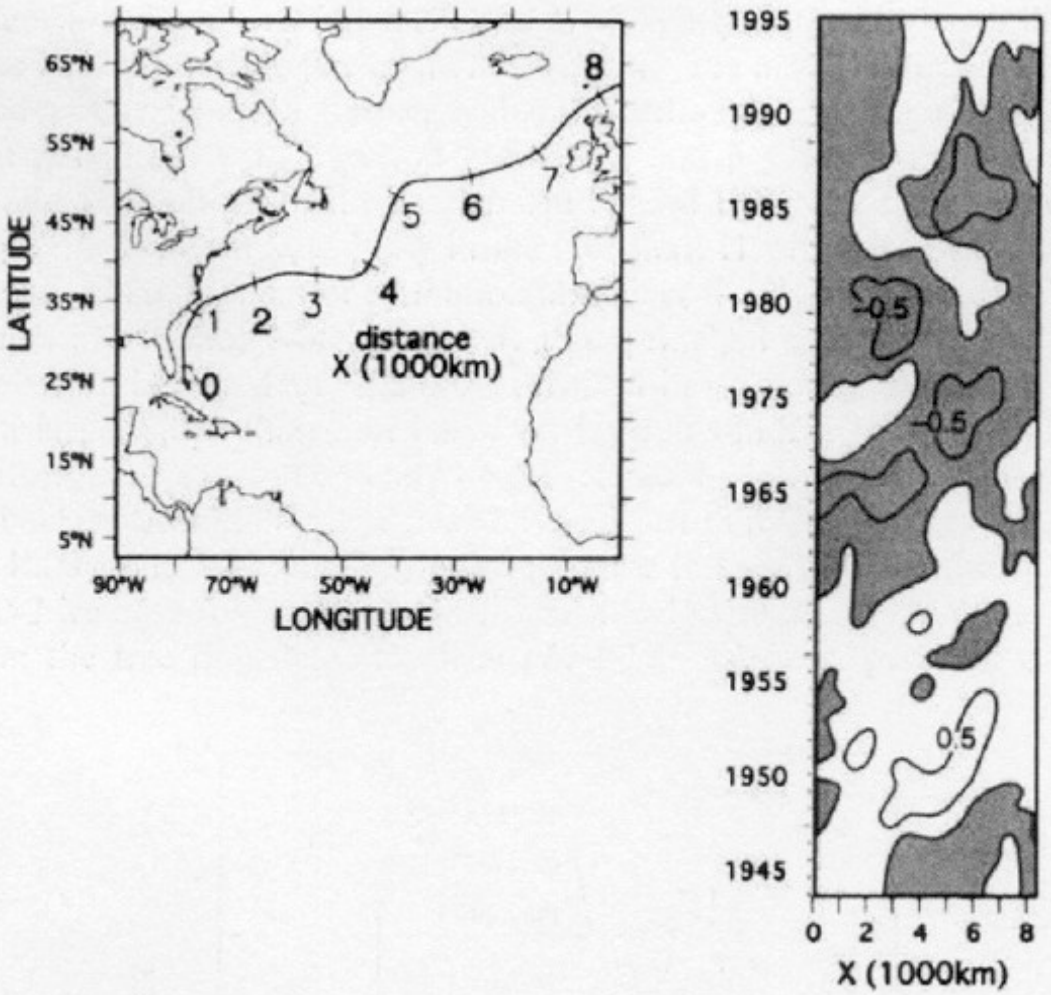

Figure 4. Left panel: pathways of interannual propagation of SST anomalies along the North Atlantic Current. Sutton and Allen (1997) find that it takes 12–14 years to travel from 0 to 7500 km, yielding an average speed of 1.7 cm s^{-1}. Right panel: Hovmoller diagram of winter SST anomalies as a function of time and position along the pathway marked on the left panel. The contour interval is 0.5°C and negative values are shaded. Modified from Sutton and Allen (1997), reproduced with permission of Nature


75°N
60°N
45°N

Impact on sea ice

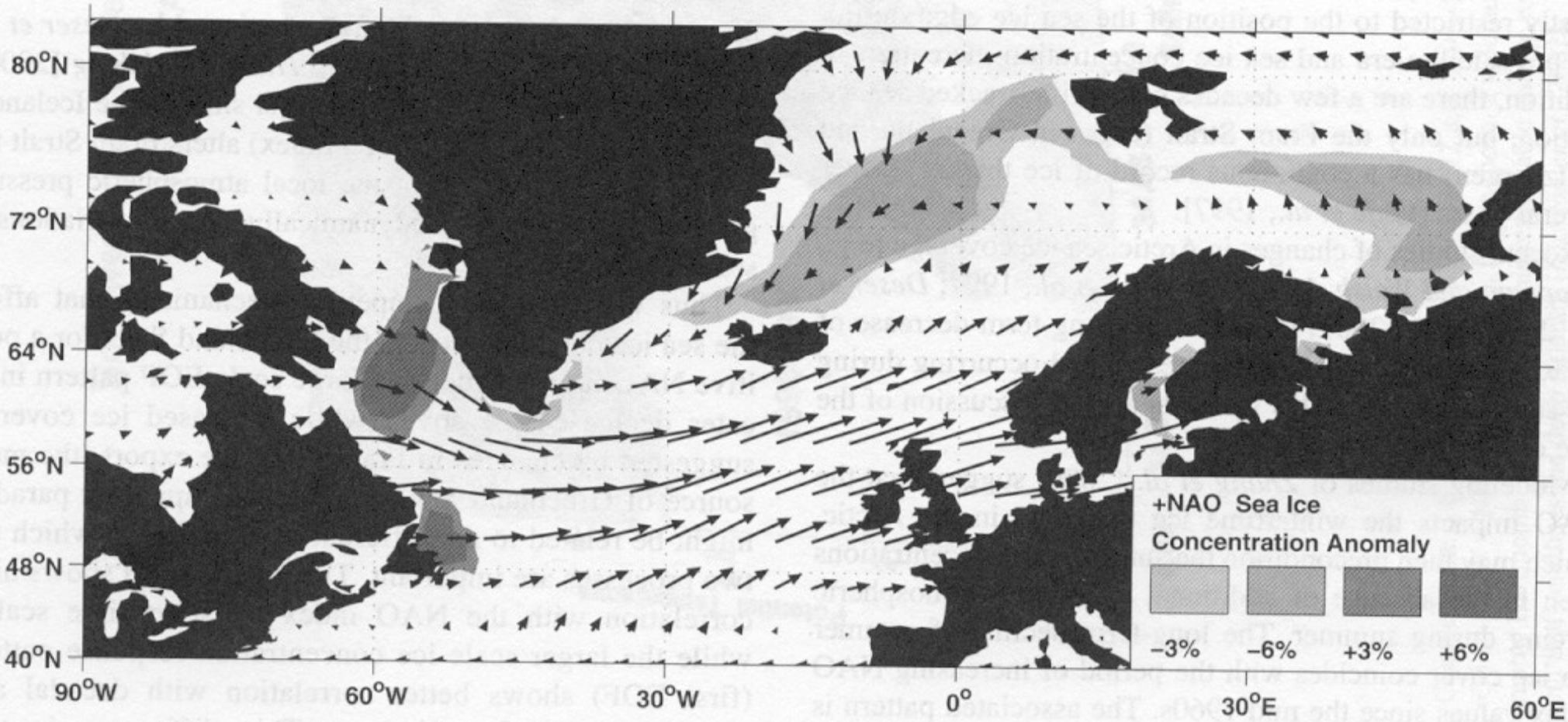

Figure 9. Winter (JFM) Arctic sea ice concentration from 1950 to 1995 [*Chapman and Walsh*, 1993] regressed onto the NAO index. Contoured are 3 and 6% changes in ice concentration. The arrows are the winter wind anomaly regressed onto the NAO index (see also Figure 3). The darker patches show increased ice concentration during a positive NAO index winter while the lighter patches show the areas where ice concentration is reduced. The sea ice concentration response to the NAO shows a pronounced seesaw pattern between the Labrador and Nordic Seas.

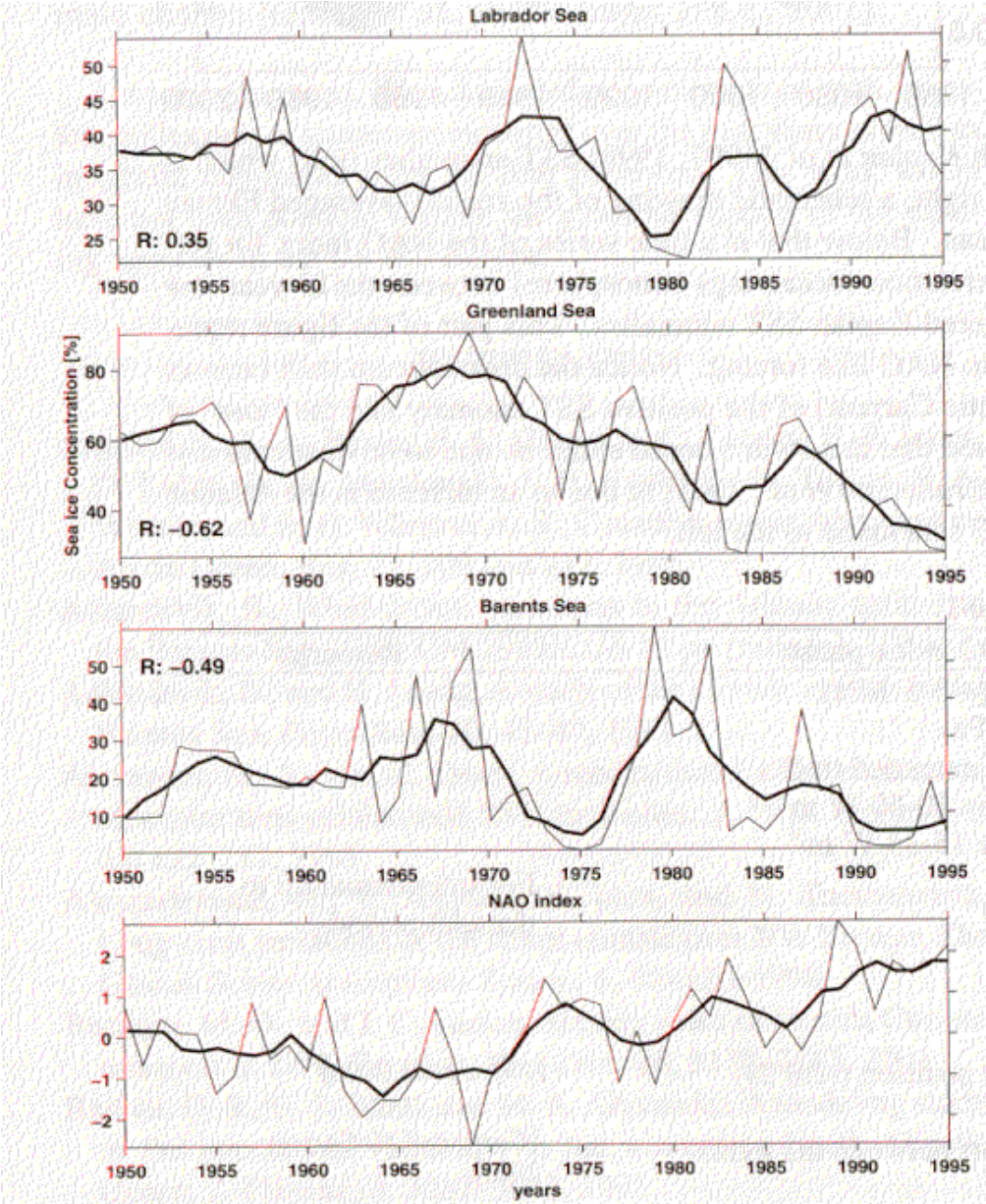

Figure 10. Time series of winter (JFM) sea ice concentration [*Chapman and Walsh*, 1993] area averaged for the Labrador Sea, Greenland Sea, and Barents Seas as well as the NAO index (lower panel). The heavy lines are obtained with a 5-year running mean filter. For each region the correlation coefficient with the NAO index is given and ranges from r=0.35 in the Labrador Sea to r= -0.62 in the Greenland Sea region.

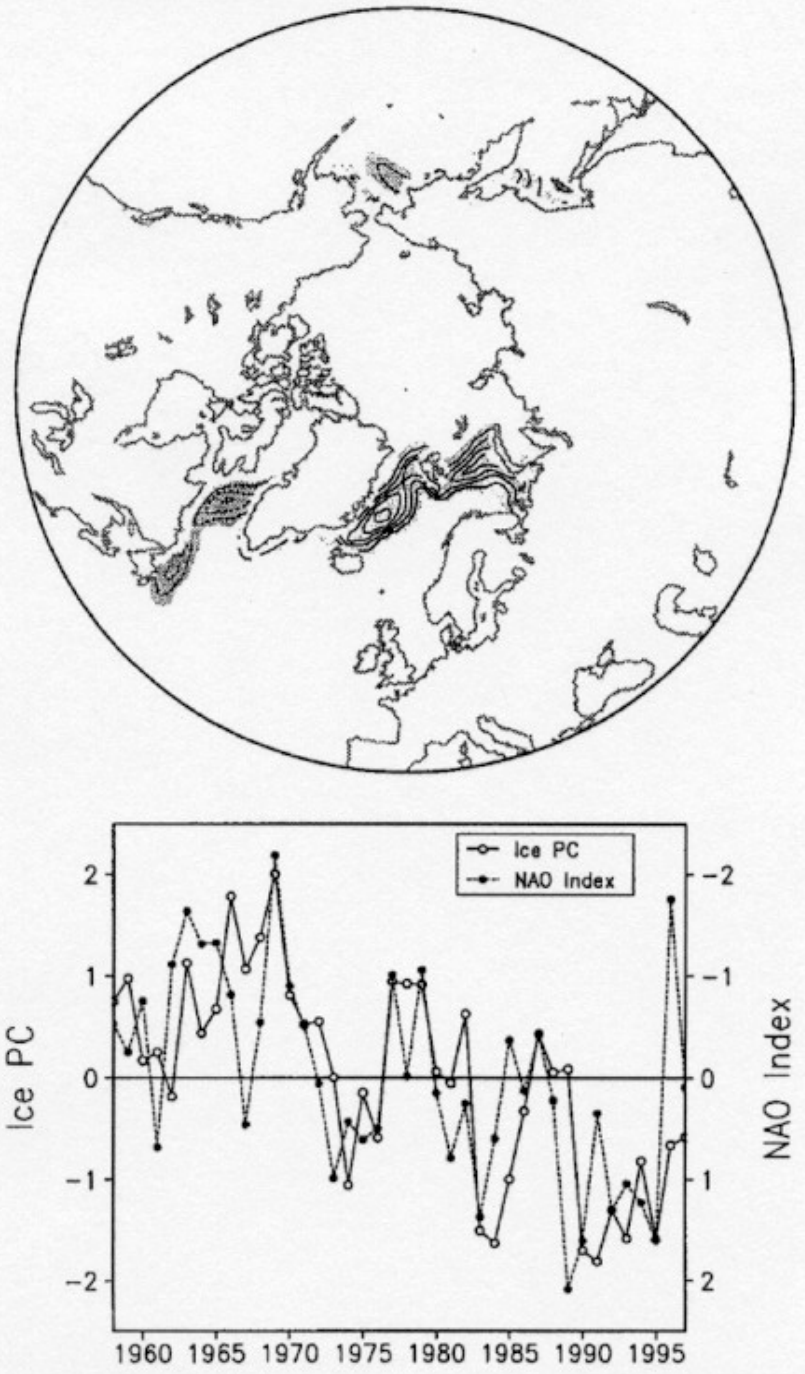

Figure 10. Top panel: leading EOF of winter sea ice concentration anomalies during 1958–1997. Contour interval is 5%, zero contour has been omitted and negative anomalies are dashed. Bottom panel: standardized time series of the first EOF of sea ice shown above (solid line) and the wintertime NAO index (scale inverted). Thus, when the NAO is low, winter sea ice concentration is anomalously high over Greenland and anomalously low over the Labrador Sea. Both panels are from Deser *et al.* (2000), reproduced by permission of the American Meteorological Society

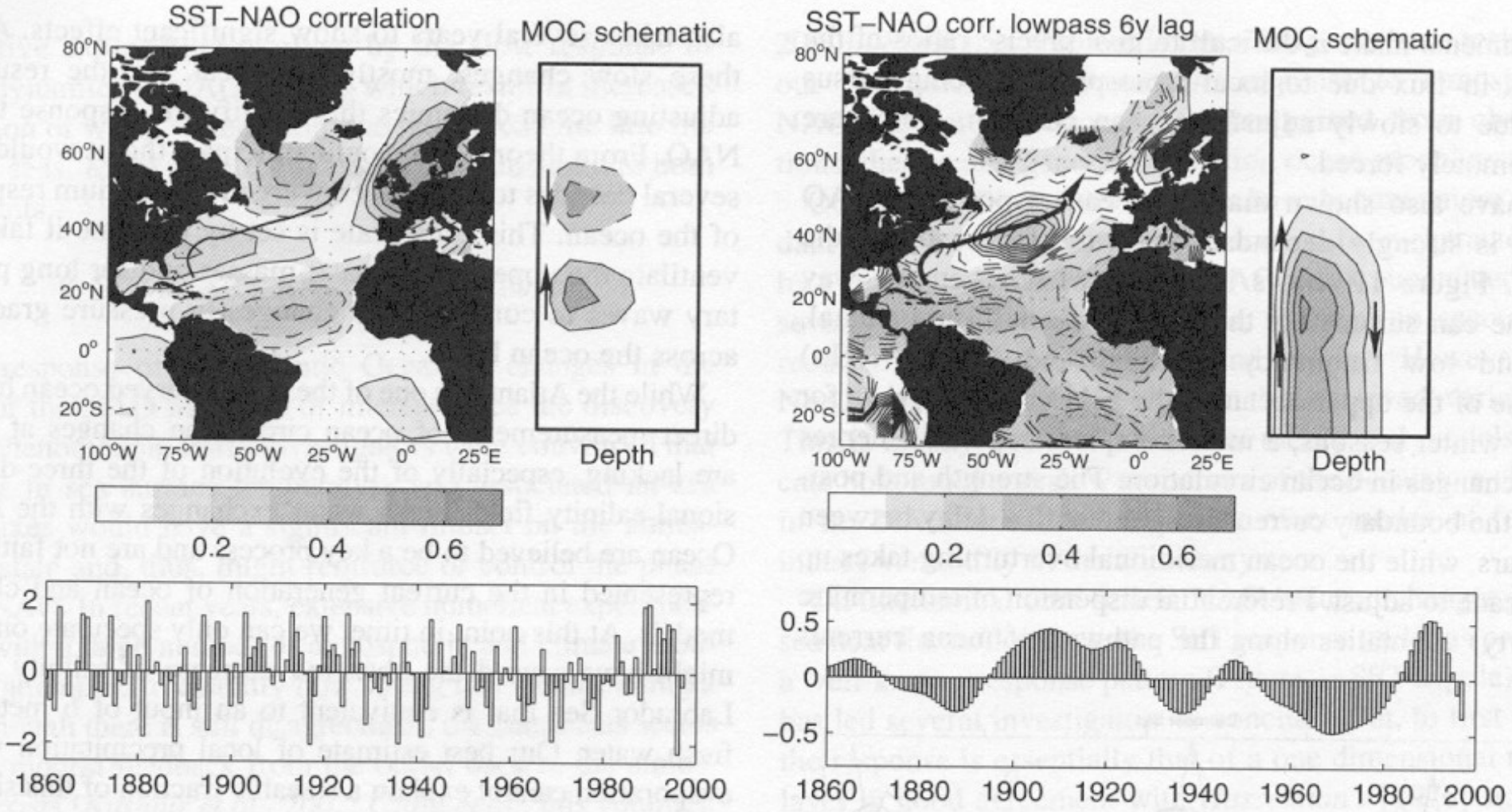

Figure 11. Correlation of the *Hurrell* [1995] NAO index with *Kaplan et al.* [1997; 1998] SST anomalies (left) which is dominated by the interannual variability. Immediately to the right, a schematic drawing of the zonally-averaged Ekman induced meridional overturning circulation (MOC) in the ocean. Below that is a time series of the NAO index for reference. The right part of the figure shows the 6 year lag correlation (ocean lags atmosphere) between the15-year low pass filtered NAO index (shown below) and the low pass filtered Kaplan SST anomalies. This part of the figure represents the decadal and lower frequency response of the ocean to NAO like forcing. Notice the down stream shift (arrows indicate position and strength of the Gulf Stream/North Atlantic Current) of the positive SST anomaly and the "loss" of the subpolar gyre cooling region. Model results have suggested that this switch could either be due to downstream dispersion of the warm temperature anomaly by the mean flow [*Krahmann et al.*, 2001] or due to an increase in the Atlantic MOC [*Eden and Willebrand*, 2001], as indicated by the MOC schematic to the left.

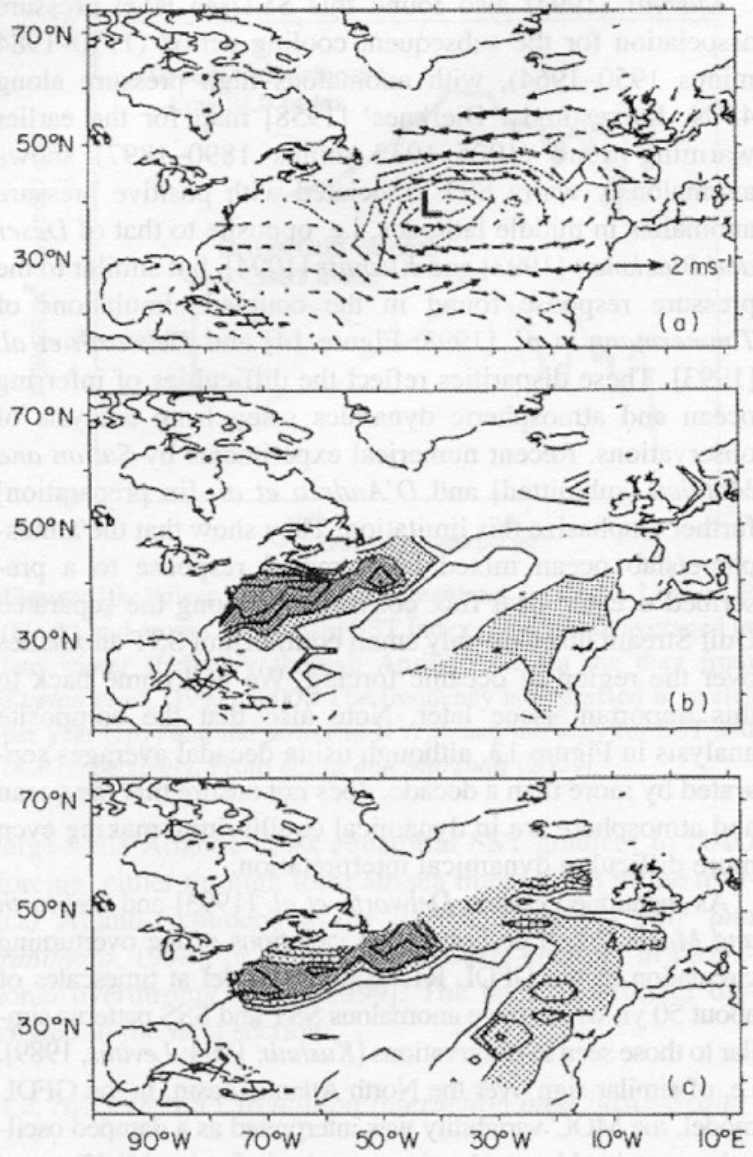

Figure 13. Difference between the periods 1939–1968 and 1900–1929 of winter (a) sea level pressure and wind, (b) SST, and (c) surface air temperature. In (a) the contour interval is 0.5 mb, with negative contours dashed. The lowest pressure anomaly is -3 mb. Wind scale is indicated in lower right. In (b) light shading indicates values between 0.8°C and 1°C; heavy shading indicates values greater than 1°C. Contour interval is 0.2°C. In (c) light shading indicates values between 0.6°C and 0.8°C; heavy shading indicates values greater than 0.8°C. Contour interval is 0.2°C. From *Deser and Blackmon* [1993; their Figure 7].

Circulation/Gulf stream response

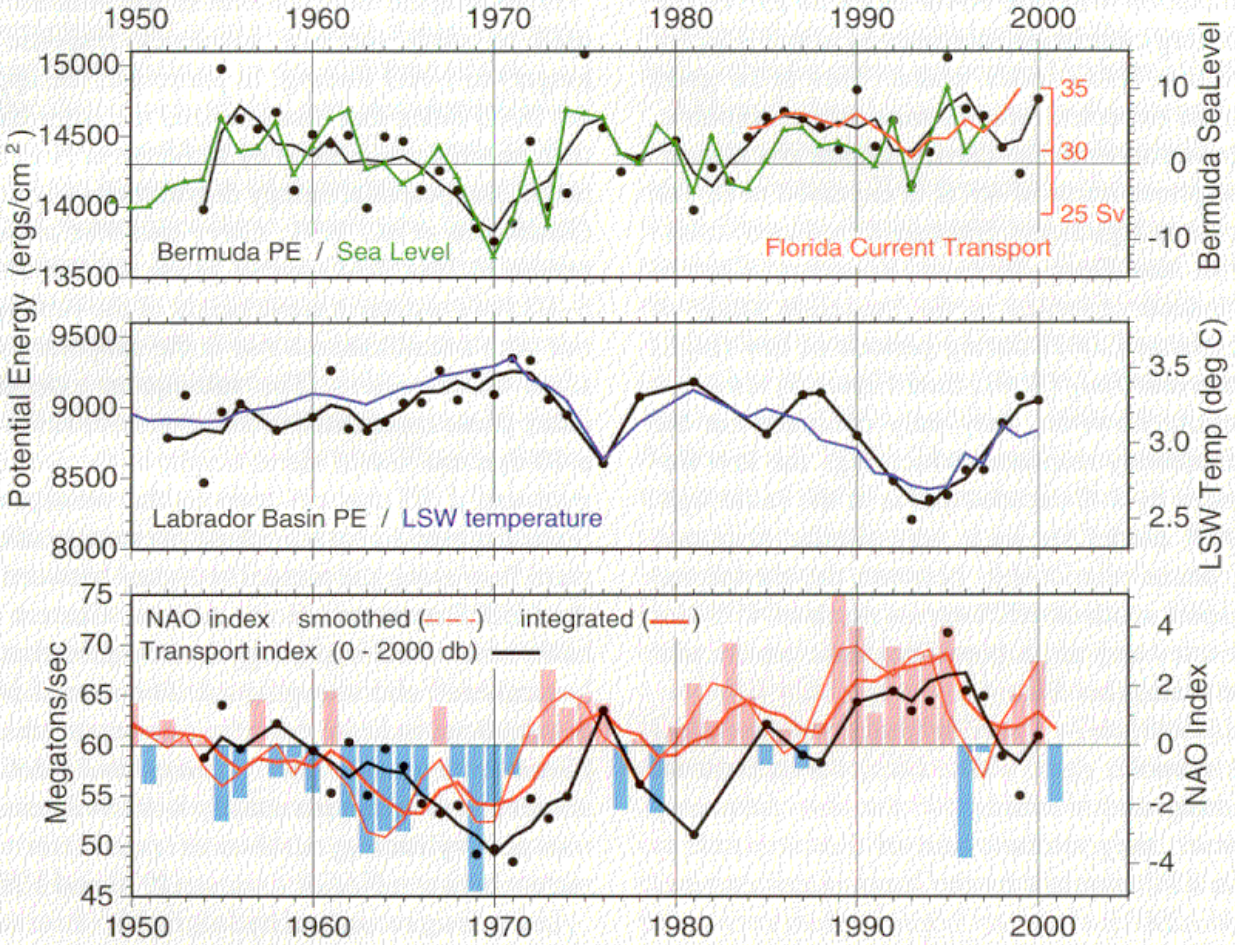

Plate 1. a) Time series of 0–2000 db potential energy at Bermuda (black circles) and smoothed with 3-point running mean (black curve). Scale is left axis. Annual sea level anomaly (unsmoothed) is portrayed by the green curve, and the scale is the right axis. Florida Current transport from *Baringer and Larsen* [2001] is the red curve and red axis. b) Time series of 0–2000 db potential energy from the central Labrador Basin (black circles and curve, as above). Temperature at 1500 db, the LSW core, is depicted by the blue curve (unsmoothed annual values) and right axis scale. c) Index of eastward baroclinic mass transport between the subpolar and subtropical gyre centers (black curve is smoothed with 3-year running mean; black circles are annual values) from *Curry and McCartney* [2001]. The pink and blue bars depict Hurrell's SLP NAO index. The red dashed curve is the NAO index smoothed with a 3-point running mean. The solid red curve is the "integrated" NAO index from *Curry and McCartney* [2001] in which each point is evaluated as the weighted sum of the 10 previous years to simulate ocean "memory."

Changes in water masses:

Subtropical mode water

Labrador Sea water

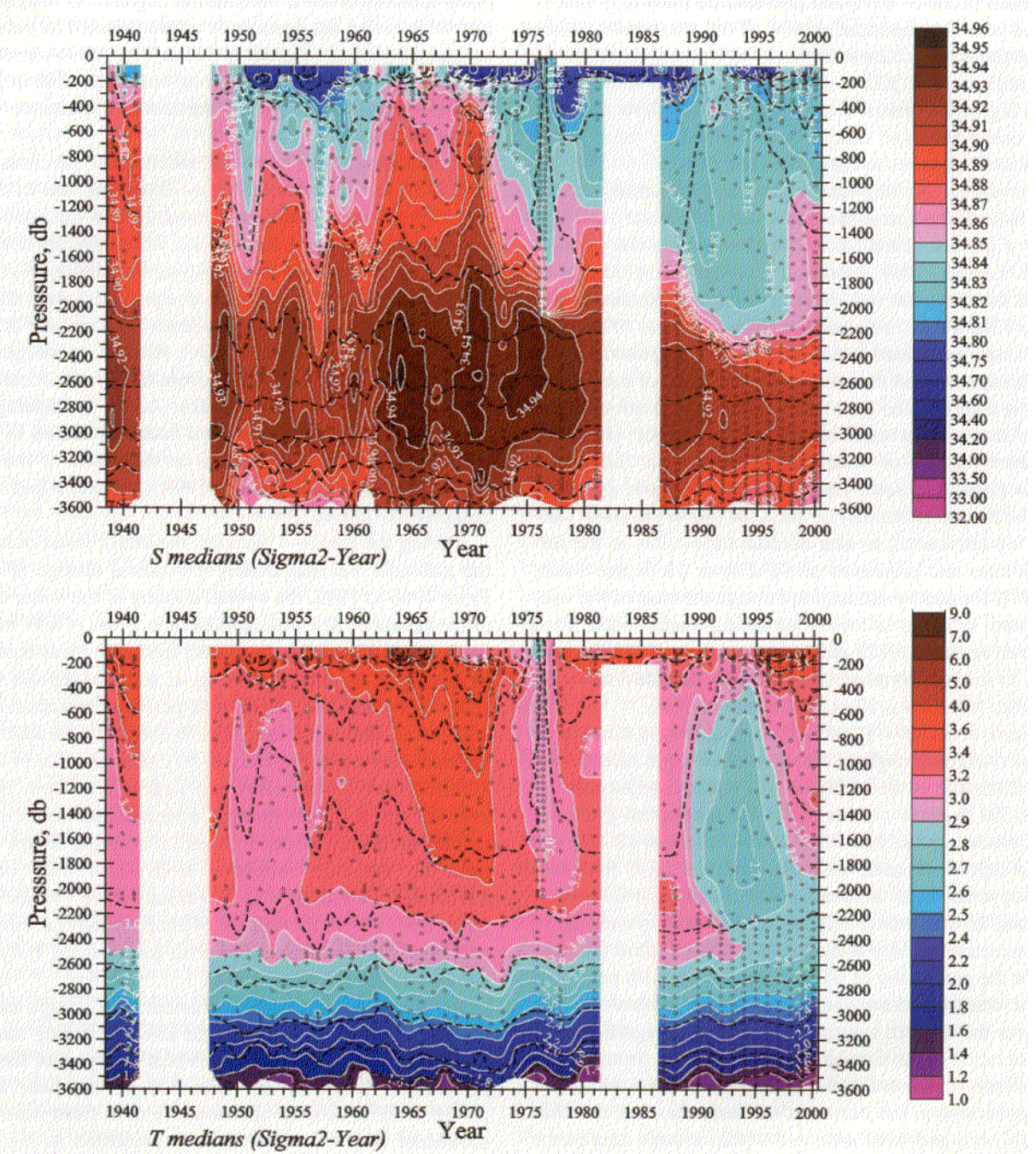

Plate 2. Changes in the salinity (upper panel) and potential temperature (lower panel) of the water column in the Central Labrador Sea over the complete period of the hydrographic record since 1938. The data set was selected to lie within the 3300 m isobath of the Labrador Sea, and the plots represent the median values of vertical property profiles, binned according to σ_{t2} density intervals. Figure was kindly provided by Igor Yashayaev, Bedford Institute of Oceanography, Dartmouth, N.S., Canada.

Changes in water mass characteristics

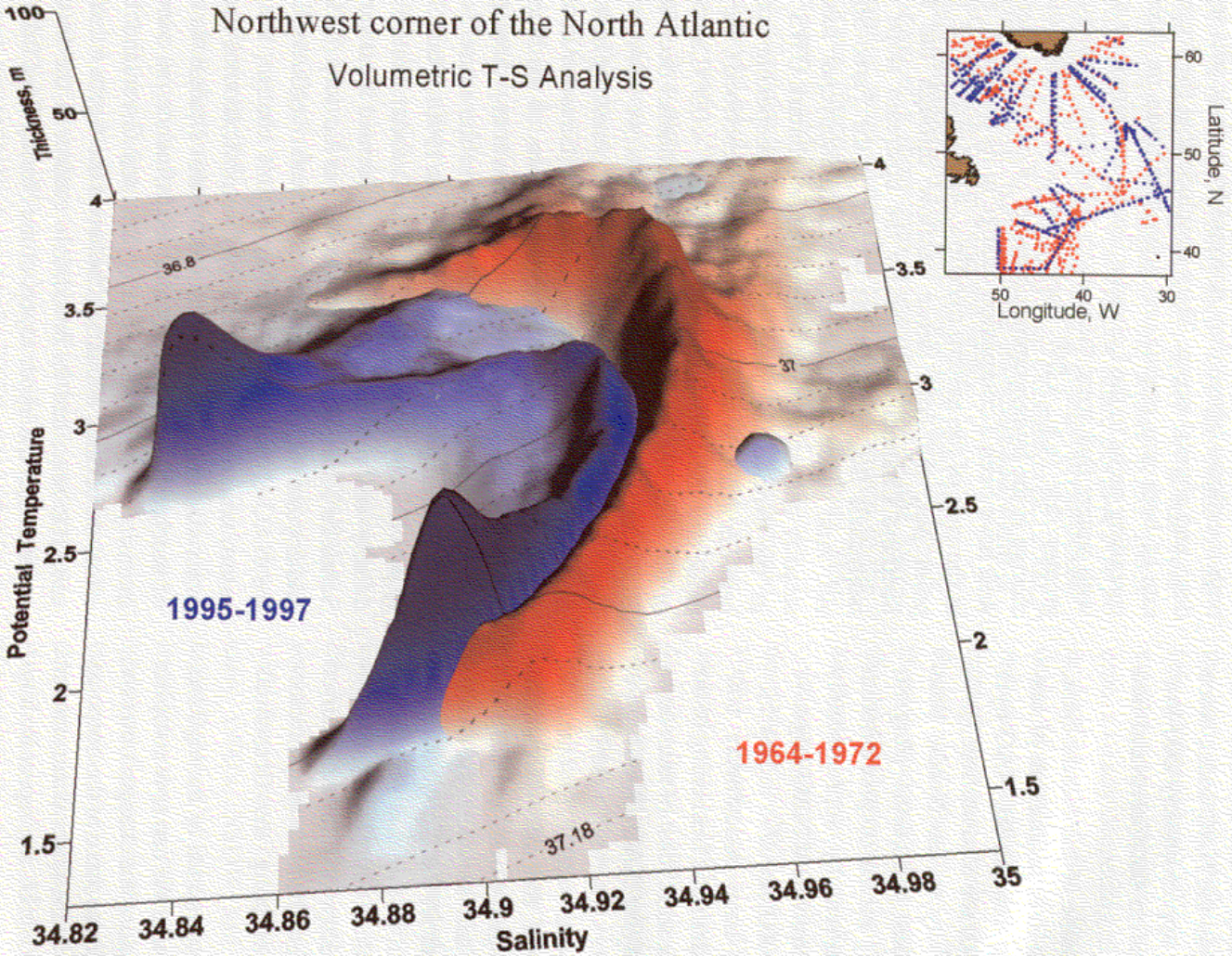

Plate 3. Change in the T-S relation between 1964–1972 and 1995–1997 for deep waters of the NW Atlantic (38°-64°N, 12°-52°W) denser than σ_{t2} =36.84 (LSW + NEADW + DSOW). Figure shows a volumetric T-S analysis kindly provided by Igor Yashayaev, Bedford Institute of Oceanography, Dartmouth, N.S., Canada. This remarkable change reflects the multi-decadal freshening of the entire system of overflow and entrainment that ventilates the deep Atlantic [*Dickson et al.*, 2002].

Summary of ocean changes to NAO forcing

Table 1.

Property	High NAO index phase	Remarks
SLP subtropical High	Stronger subtropical High (+ 3-5 hPa)	
SLP Icelandic Low	Deeper polar Low (- 7-9 hPa)	
Storm tracks	More northeasterly tilt and extended tracks	
Heat flux over subpolar gyre	Enhanced ocean heat loss by 20-50 W m^{-2}	
Heat flux over subtropical gyre	Reduced ocean heat loss by 15-35 W m^{-2}	
SST within subpolar gyre	0.5-1.0 °C colder	For interannual up to decadal periods.
SST western subtropical gyre	0.3-0.7°C warmer	
SST northeastern tropical Atlantic	0.4-0.8°C colder	
Gulf Stream position	20-50 km north of its mean position (~39°N) between 70-60°W	[*Joyce et al.* 2000]
Baroclinic transport (Labrador Sea - Bermuda)	Enhanced eastward transport between the gyres by 5-9 Sv	[*Curry and McCartney* 2001]
Thickness change of Labrador Sea Water	50-100 m increase per year of forcing	[*Curry et al.* 1998]
Transport of Florida Current	Reduced by 1-2 Sv out of a mean of 32 Sv	[*Baringer and Larsen,* 2001]
Ice cover in Labrador Sea	Enhanced	[*Deser et al.* 2000]
Ice cover in Greenland Sea	Reduced	[*Deser et al.* 2000]
Deep mixing (convection) in the Labrador Sea	Enhanced up to 2500m maximum depth	[*Dickson et al.* 1996; *Lazier* 1995]

Does the atmosphere respond to the NAO induced SST anomalies?

Conclusion of these AGCM simulations with observed SST boundary forcing are controversial, see Bretherton and Battisti 2000.

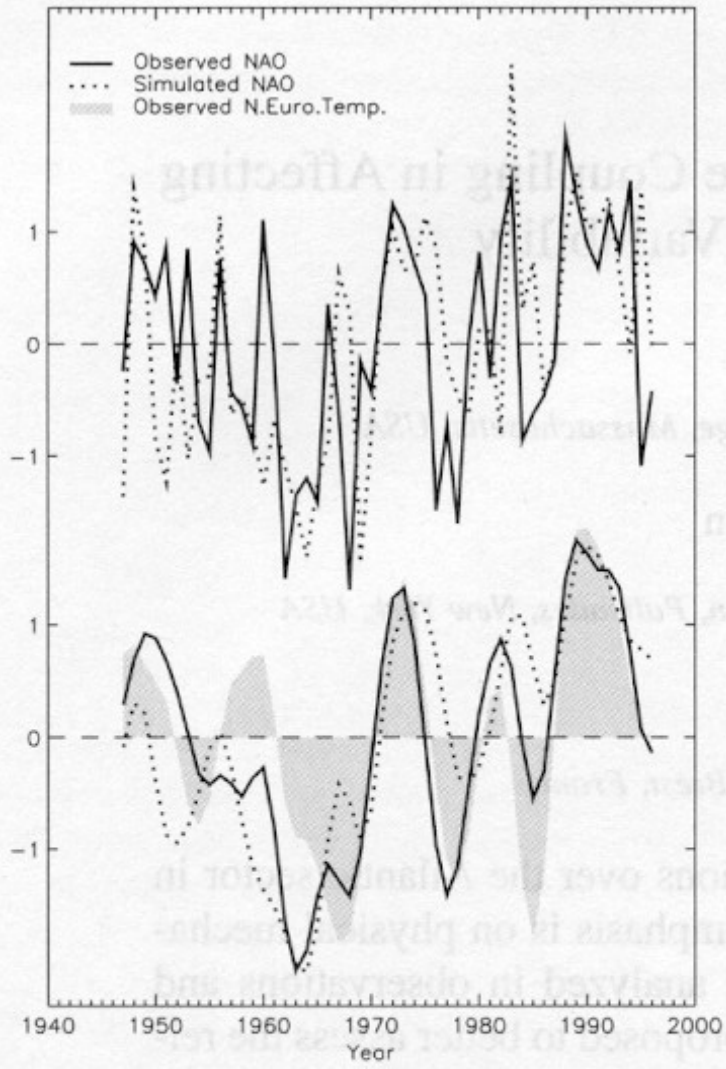

Figure 1. Observed (solid line) and modeled ensemble average (dotted line) of the *normalized winter* (DJF) NAO index. The lower graph shows the normalized NAO index time series after they have been filtered to pass variations with periods greater than 6.5 years. Shading in lower graph is the normalized filtered time series of observed North European surface temperature (averaged over 5–50°E, 50–70°N). The year corresponds to December for each DJF season. From *Rodwell et al.* [1999].

Covariability of oceanic and atmospheric temperatures

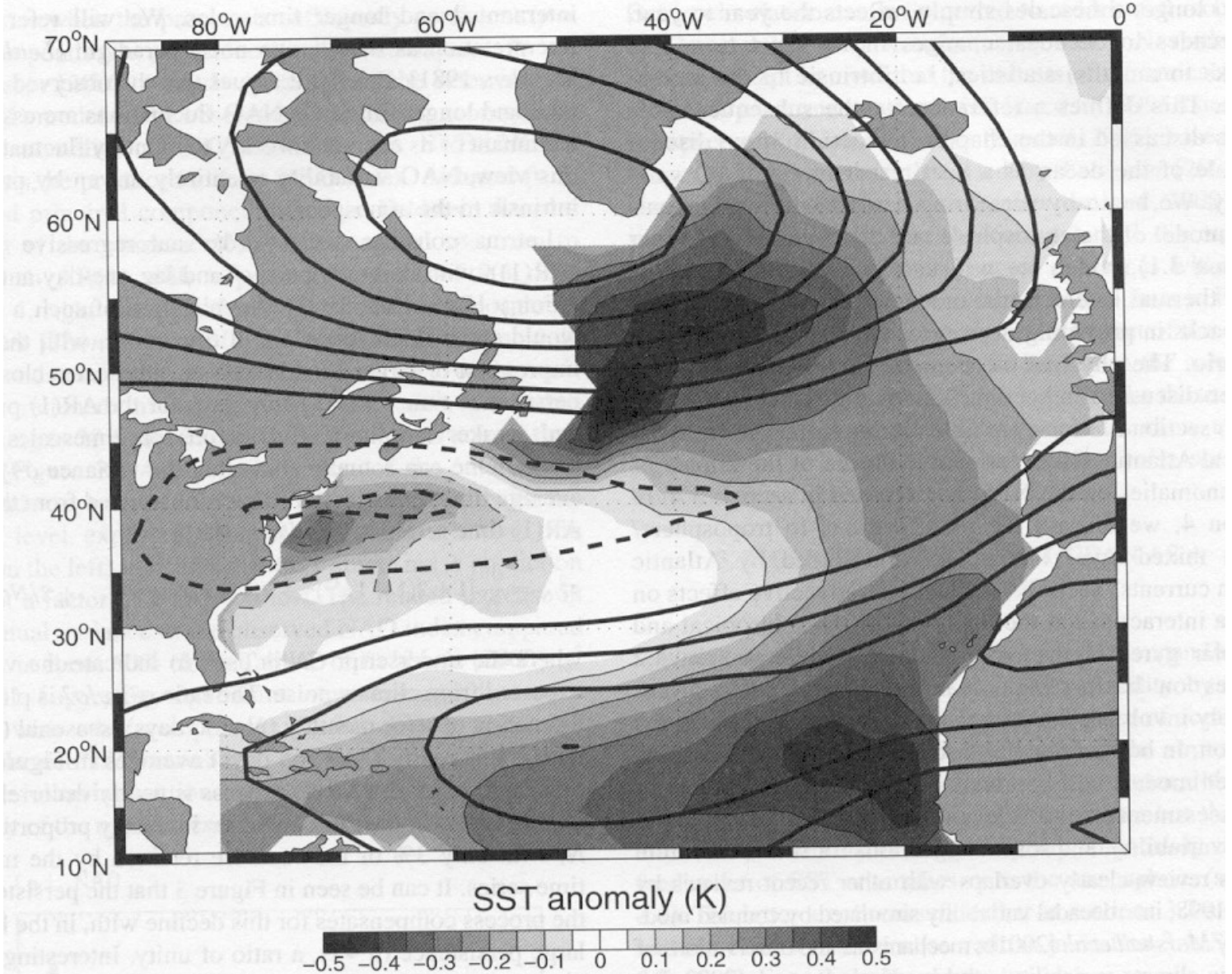

Figure 2. Dominant pattern of covariability between monthly temperature at 500 mb (contoured every 0.1 K, dashed when negative) and SST (shaded with dashed contours when negative). Anomalies from the NCEP/NCAR reanalysis data (1958–1999), as found in a maximum covariance analysis [also called SVD in the literature, see *Bretherton et al.*, 1992]. The mode explains 55% of the square covariance between the temperature fields. All months were considered in the analysis, not only wintertime.

Reddening of atmospheric spectra

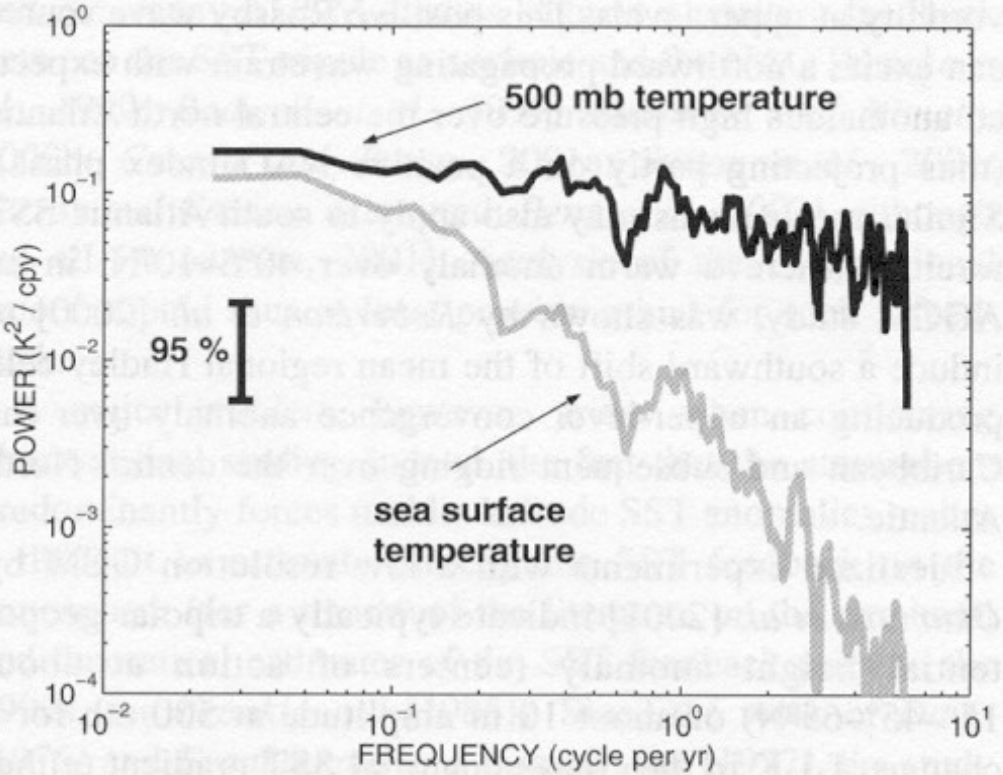

Figure 7. Power spectrum of atmospheric temperature at 500 mb (black) and SST (grey) time series associated with the spatial patterns in Figure 2. The monthly time series were scaled to represent a basin-average amplitude. The frequency is expressed in cycles per yr (*cpy*), and the power in K^2/cpy. The spectra of the linearly detrended time series were estimated using the multitaper method [*Percival and Walden*, 1993] with 9 tapers. The vertical bar indicates the 95% confidence level.

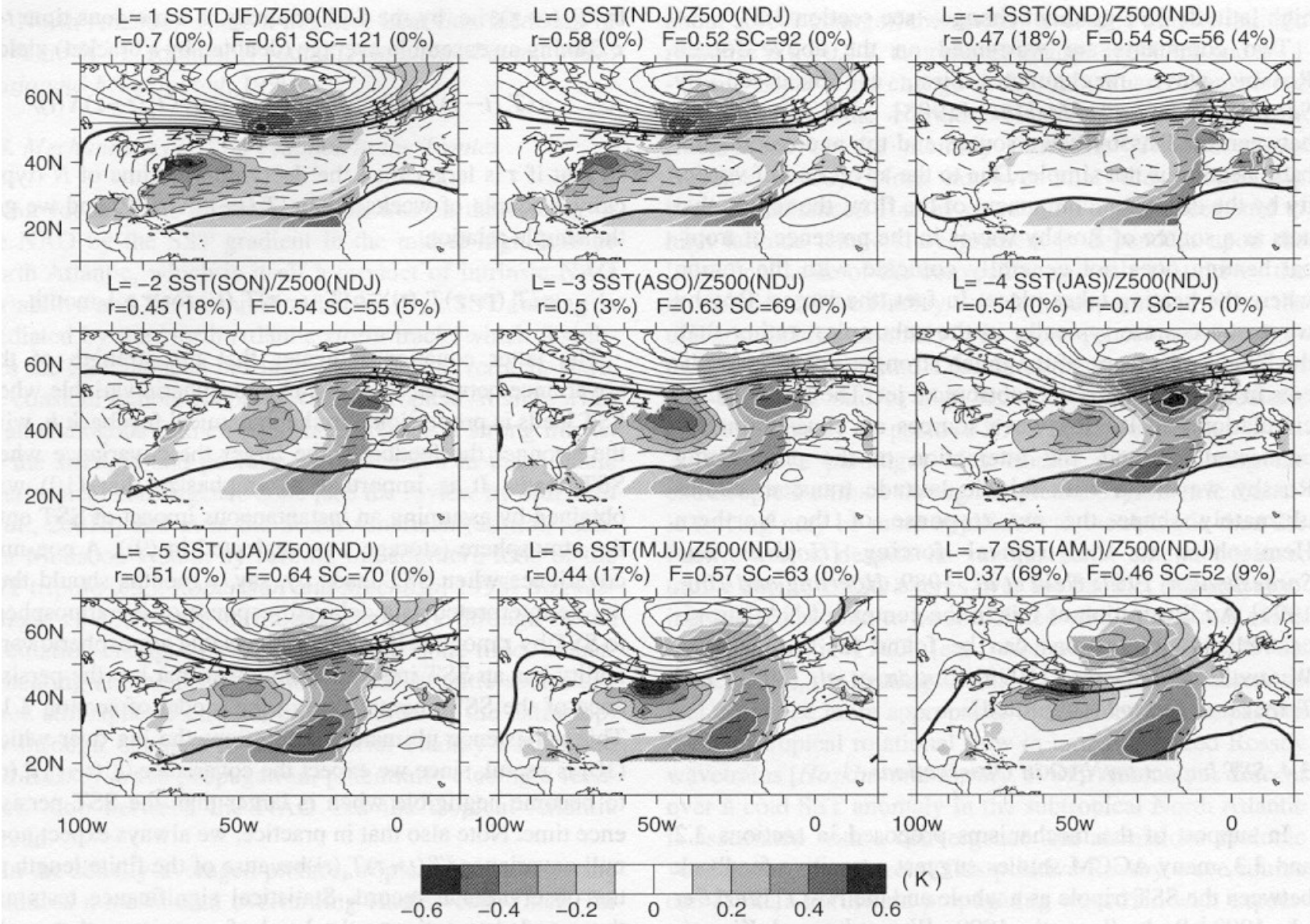

Figure 8. Dominant patterns of covariability between monthly SST (in *K*, shaded with white contours when positive) and 500 mb height (contoured every 5 m, continuous when positive) anomalies. The height field is fixed to November through January and the SST field lagged accordingly by *L* months, as indicated on the plot (SST leads when $L < 0$). Also indicated are the temporal correlation coefficient *r*, the fraction of squared covariance *F* explained by the patterns, and their squared covariance *SC*. The number in parenthesis indicates a significance level (percentage of chance that the observed covariance arise by chance), as deduced from Monte Carlo simulations. From *Czaja and Frankignoul* [2002].

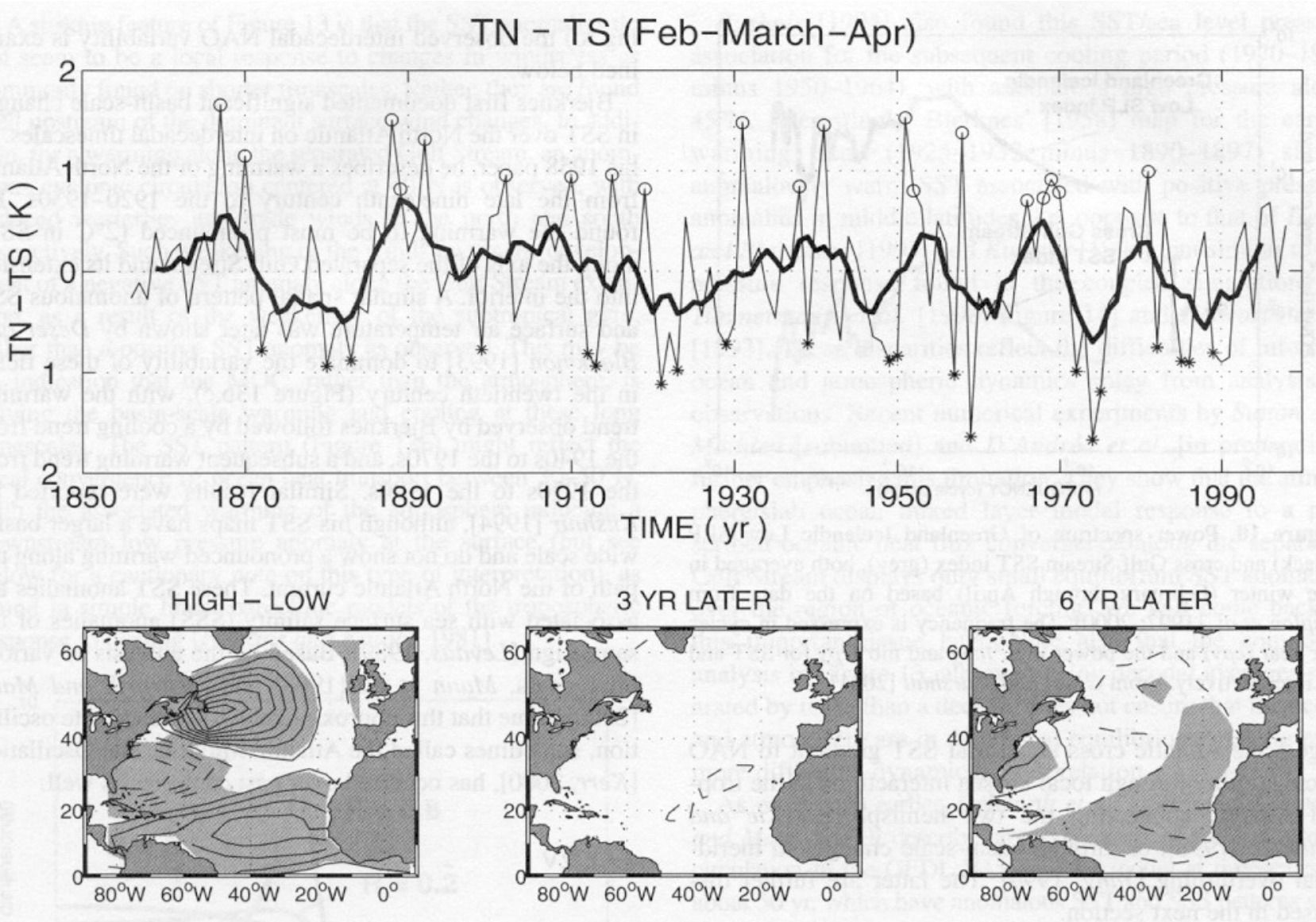

Figure 9. (upper panel) Time series of the cross Gulf Stream SST index ΔT (in K, February through April averaged, raw time series thin, 6-yr running mean thick). (bottom panel) Composite maps for SST anomalies, based on years where the ΔT index is high and low, as indicated by the circles and stars in the upper panel. The left panel indicates the large-scale SST anomalies associated simultaneously with $\Delta T > 0$, while the middle and right panels indicate the SST anomalies 3 years and 6 years after strong $\Delta T > 0$ events. The SST anomalies are contoured every 0.2K (dashed when negative), and the shading indicates where the composites are significant within the 95% confidence level, as deduced from a Student t-test. All SST data are from *Kaplan et al.* [1997]. From *Czaja and Marshall* [2001].

Czaja and Marshall suggest that the enhanced variability results from coupled feedbacks between SST, SLP and the Gulf stream

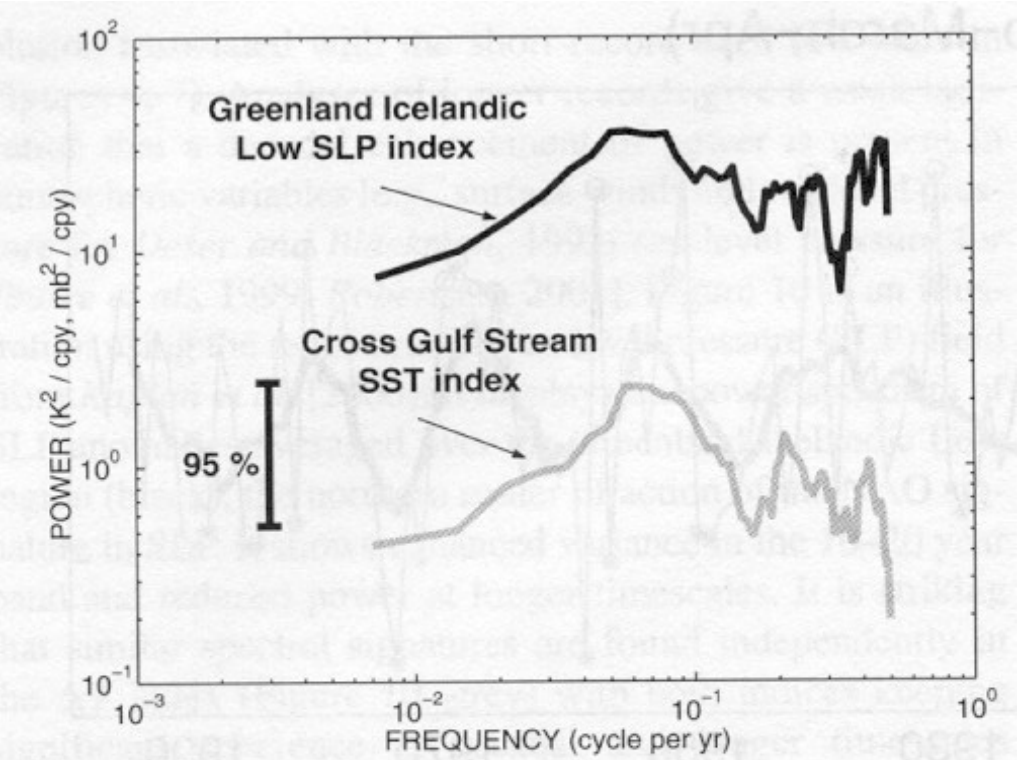

Figure 10. Power spectrum of Greenland Icelandic Low SLP (black) and cross Gulf Stream SST index (grey), both averaged in late winter (February through April) based on the data from *Kaplan et al.* [1997; 2000]. The frequency is expressed in cycles per year (*cpy*) and the power in K^2/cpy and mb^2/cpy for SST and SLP respectively. From *Czaja and Marshall* [2001].

Possible link to thermohaline circulation

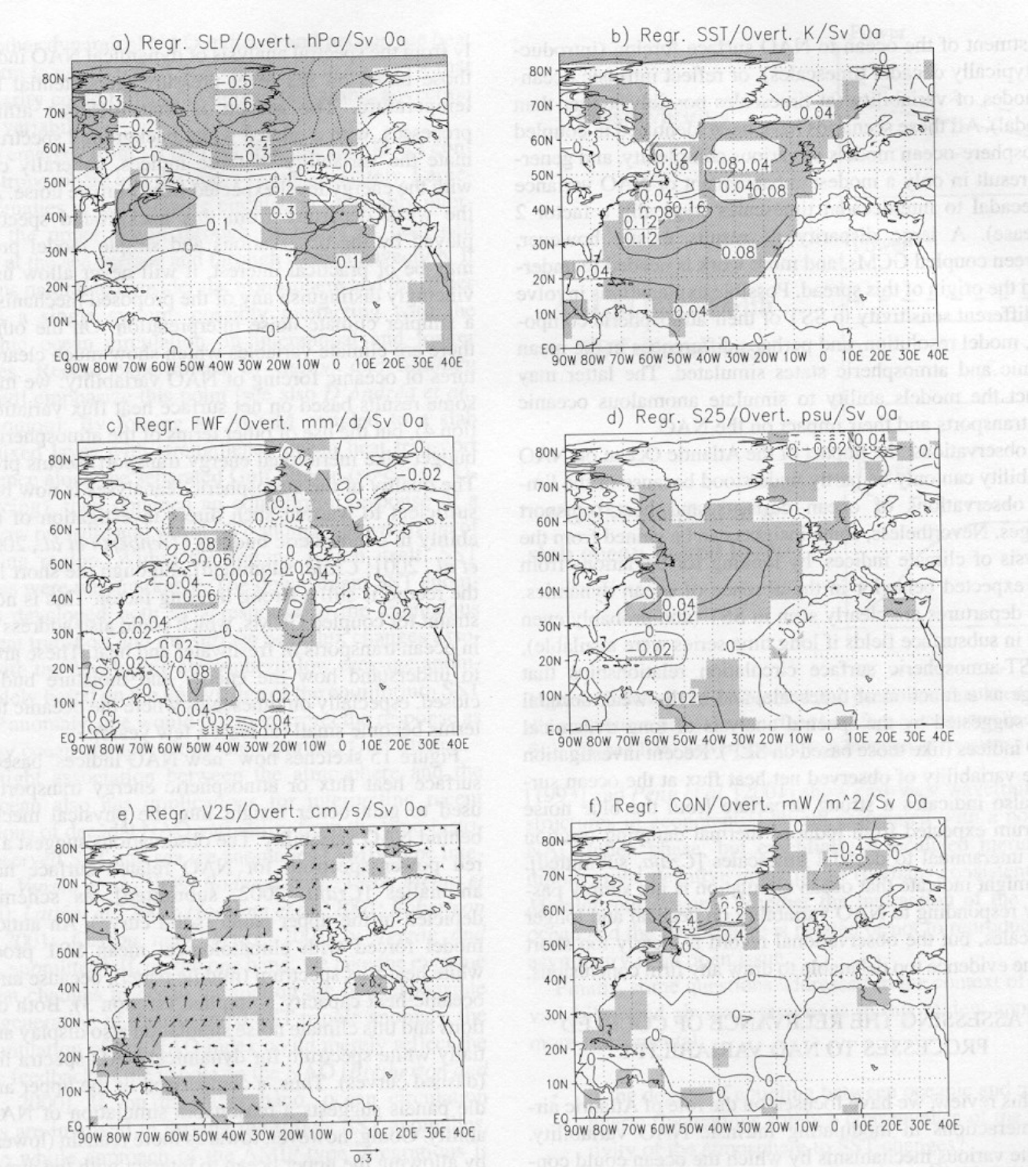

Figure 14. Simultaneous regression map of various quantities onto a band-passed (25–45 years) filtered meridional overturning index. See text for a description. From *Timmermann et al.* [1998; their Figure 14].

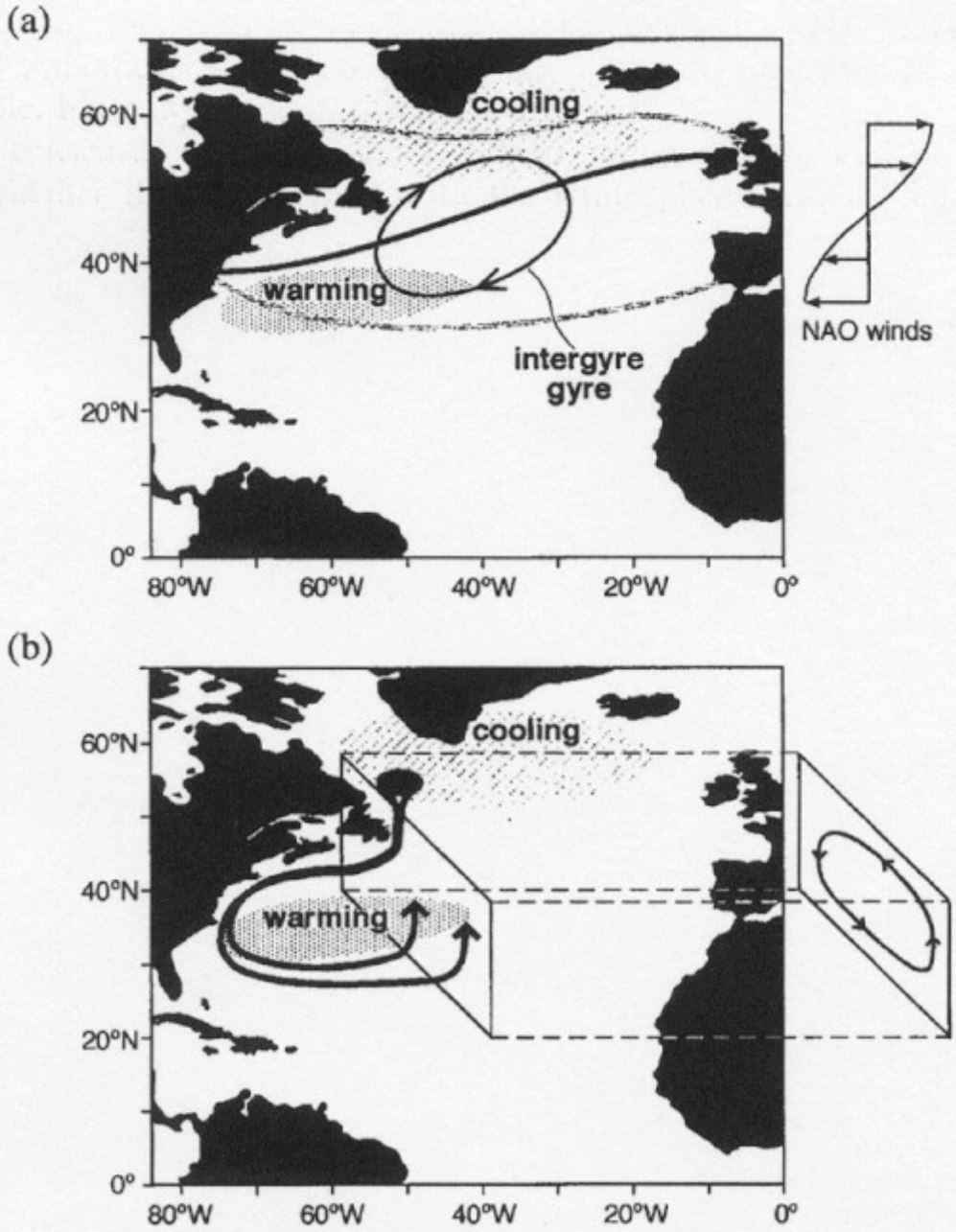

Figure 13. (a) Schematic diagram of the wind stress curl and air–sea flux anomaly patterns associated with a positive NAO. We see a 'Z' whose diagonal is the zero wind-curl line of the climatology and whose top and bottom are the zero wind-curl lines of the NAO anomaly shown in Figure 2(c). Regions of warming and cooling of the ocean due to the air–sea flux anomalies shown in Figure 2(b) are indicated. The sense of the wind-driven 'intergyre' gyre spun up by NAO(+) wind-curl forcing is also shown. (b) Schematic diagram of the anomaly in thermohaline circulation induced by the dipole in ocean thermal anomalies created by anomalies in air–sea heat fluxes associated with NAO(+) shown in Figure 2(b). The imagined anomaly in overturning circulation sketched in the meridional section on the right represents a zonal average picture

Tropical Atlantic Variability

Leading EOF of tropical Atlantic SST

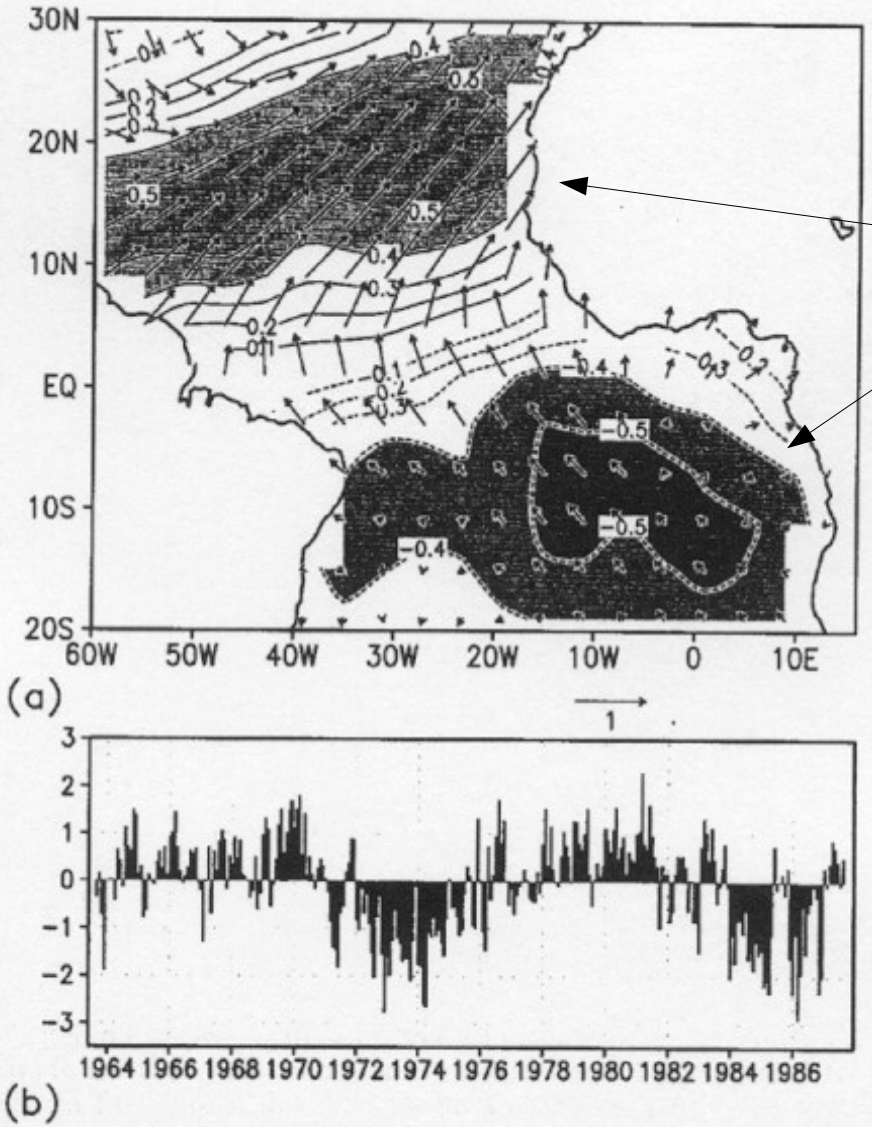

Note that N and S SST indices are poorly correlated

Figure 6. The dominant pattern of tropical Atlantic variability revealed by a joint EOF analysis of surface wind stress and SST monthly anomalies, September 1963–August 1987. Spatial structures of the first EOF mode and the associated time coefficients are illustrated in (a) and (b), respectively. Contours represent SST loading values, interval of 0.1°C. Vectors depict wind stress loadings. The unit vector represents an easterly wind stress anomaly of 1.0 dyn cm^{-2}. The time coefficients have been normalized by their own standard deviations. From Nobre and Shukla (1996), reproduced by permission of the American Meteorological Society

Correlation of SST and precipitation with Tropical Atlantic Dipole

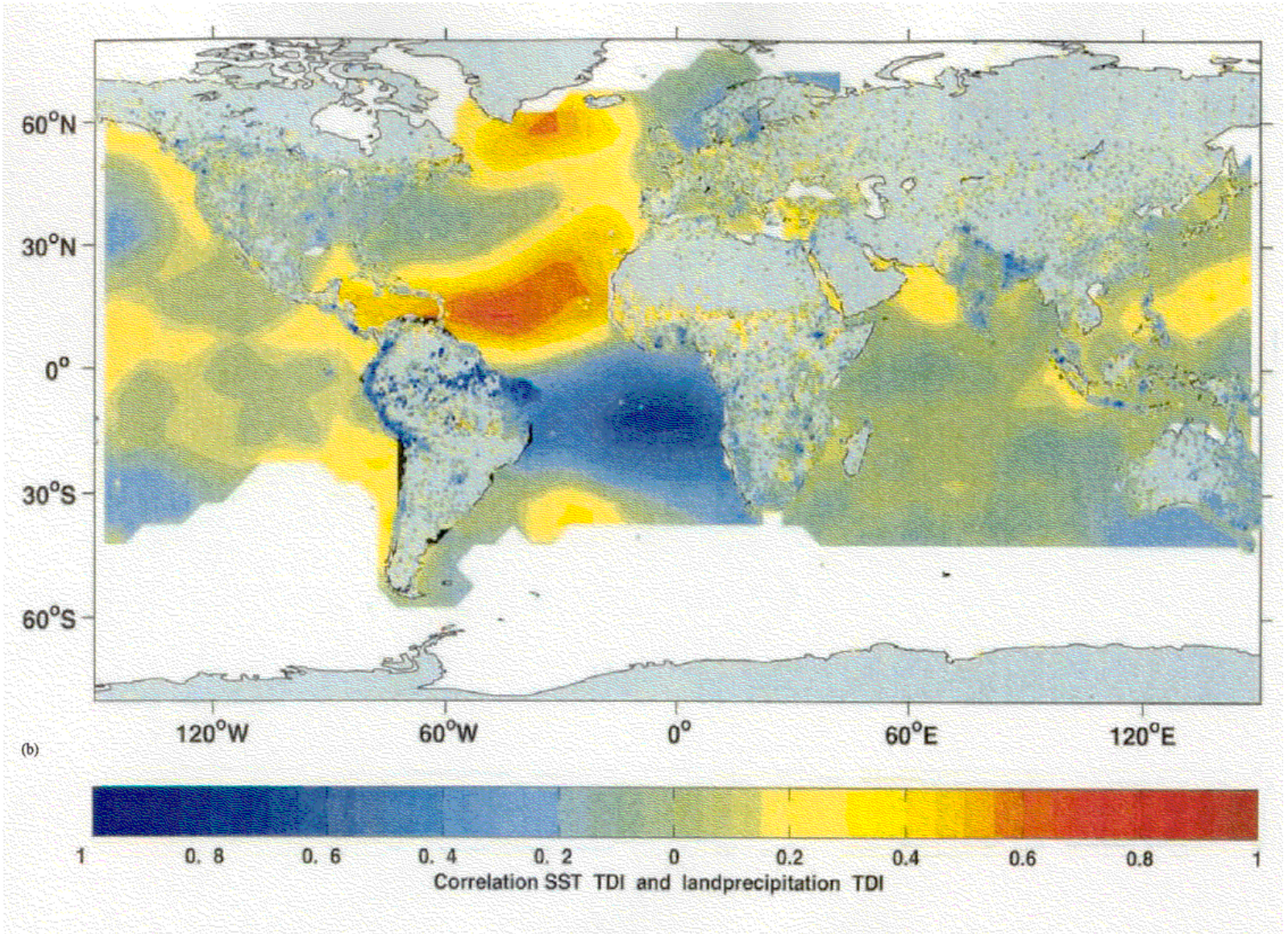

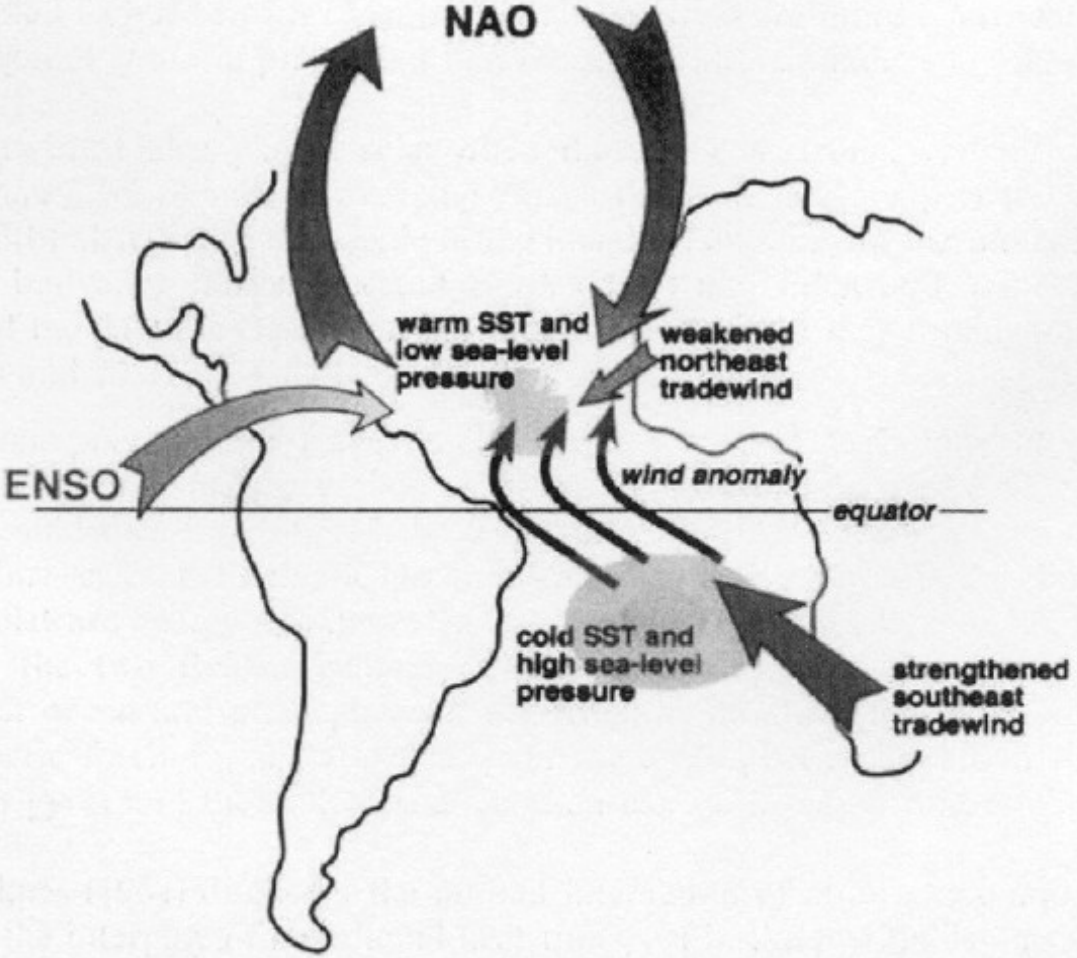

Figure 15. SST anomalies north of the equator are subject to remote influence from the NAO itself and from ENSO-related variability in the tropical Pacific. In response to a positive north–south SST difference anomaly, northward cross-equatorial winds shift the position of the ITCZ, act to reduce the northeasterly mean trade winds in the north and enhance the southeasterly trades in the south. The resulting anomalous heat flux tends to reinforce the initial north–south SST difference, which in turn strengthens the cross-equatorial wind anomalies. Negative feedbacks, perhaps due to horizontal heat transport by ocean currents, may counteract the unstable air–sea interaction yielding a self-sustained oscillation. The resulting variability of the ITCZ could influence the NAO to the north through rearranging the Hadley circulation

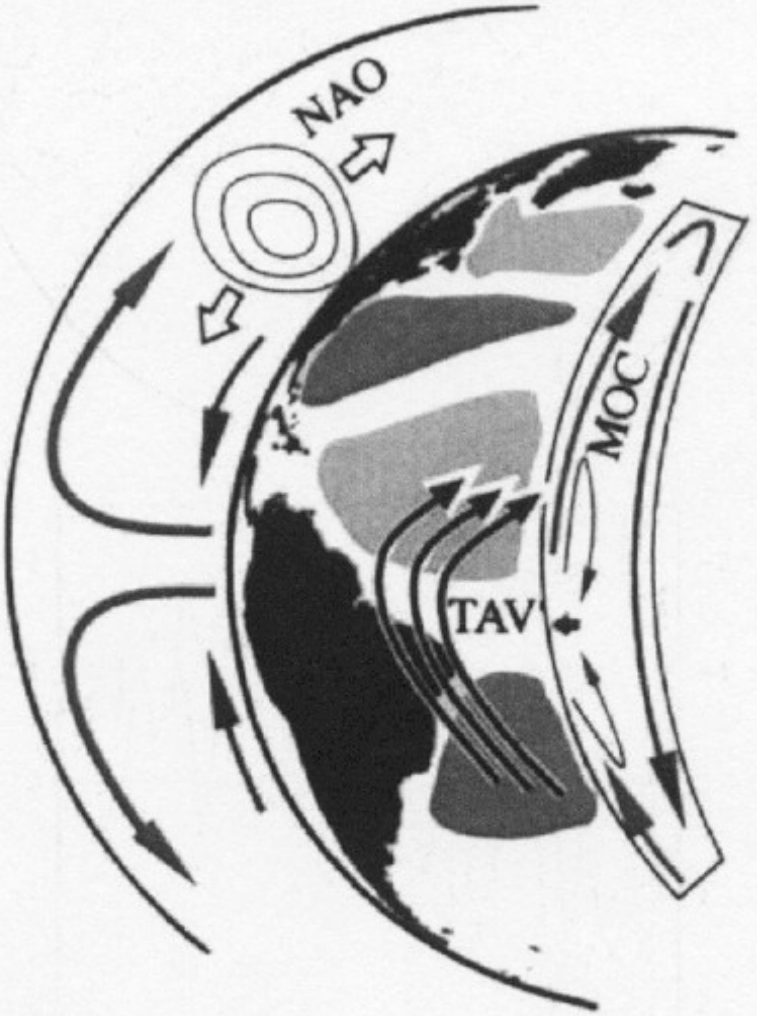

Figure 12. A schematic of TAV ⇆ NAO ⇄ MOC interactions. The NAO, reaching down into the tropics and up to high latitudes, is an important source of variability for TAV and the MOC. In turn, the TAV through its influence on tropical/subtropical SSTs can feedback on the NAO through the Hadley circulation. The MOC, a major contributor to meridional heat transport, can also affect the magnitude of the pole–equator temperature gradient over the Atlantic sector, the strength of the mid-latitude jet stream and hence the NAO. Extending high up into the stratosphere, the NAO may also influence, and be influenced by, the strength and position of the polar stratospheric vortex. The strength of the coupling between the NAO and the stratosphere above and the ocean below is not yet clear